Universidade de Lisboa
Faculdade de Ciências
Departamento de Física

THE LARGEST LYα NARROW BAND SURVEY AT Z = 5.7: IMPLICATIONS FOR REIONIZATION

Mestrado em Física
Especialização em Astrofísica e Cosmologia

Sérgio Miguel da Graça Santos

Dissertação orientada por:
Doutor David Ricardo Serrano Gonçalves Sobral

2016

Results from this work have been submitted to MNRAS, pre-print available in arxiv:1606.07435 (Santos et al., 2016).

Abstract

We present new results from the widest narrow band survey search for Lyα emitters at $z = 5.7$, just after reionization. We survey a total of $7\,\mathrm{deg}^2$ spread over the COSMOS, UDS and SA22 fields. We find over 11,000 line-emitters, out of which 514 are robust Lyα candidates at $z = 5.7$ within a volume of 6.3×10^6 Mpc^3. Our Lyα emitters span a wide range in Lyα luminosities, from faint to bright ($\mathrm{L}_{\mathrm{Ly}\alpha} \sim 10^{42.5-44}\,\mathrm{erg\,s^{-1}}$) and rest-frame equivalent widths ($\mathrm{EW}_0 \sim 25 - 1000\,\mathrm{\AA}$) in a single, homogeneous data-set. By combining all our fields we find that the faint end slope of the $z = 5.7$ Lyα luminosity function is very steep, with $\alpha = -2.3^{+0.4}_{-0.3}$. We also present an updated $z = 6.6$ Lyα luminosity function, based on comparable volumes and obtained with the same methods, which we directly compare with that at $z = 5.7$. We find a significant decline of the number density of faint Lyα emitters from $z = 5.7$ to $z = 6.6$ (by $0.5 \pm 0.1\,\mathrm{dex}$), but no evolution at the bright end/no evolution in L^*. Faint Lyα emitters at $z = 6.6$ show much more extended haloes than those at $z = 5.7$, suggesting that neutral Hydrogen plays an important role, increasing the scattering and leading to observations missing faint Lyα emission within the epoch of reionization. All together, our results indicate that we are observing patchy reionization which happens first around the brightest Lyα emitters, allowing the number densities of those sources to remain unaffected by the increase of neutral Hydrogen fraction from $z \sim 5$ to $z \sim 7$.

Keywords: galaxies: high-redshift – galaxies: luminosity function – cosmology: observations – cosmology: dark ages, reionization, first stars.

Resumo em Português

Durante as últimas duas décadas, o nosso conhecimento sobre o Universo distante tem evoluído significativamente, beneficiando da construção de novas infraestruturas observacionais com sofisticados instrumentos na Terra (e.g. VLT, ALMA, Keck) e no espaço (e.g. HST, Spitzer). Observações directas do Universo distante são essenciais para constranger modelos cosmológicos e simulações computacionais e para obter medições mais precisas de parâmetros cosmológicos.

Actualmente as amostras de galáxias a altos desvios para o vermelho (redshift) são maioritariamente selecionadas pela sua emissão contínua no ultravioleta (UV). Devido à típica estratégia de procurar em pequenas áreas, a maioria das galáxias detectadas é extremamente ténue, o que torna estudos detalhados de galáxias individuais extremamente desafiantes, senão mesmo impossíveis com a tecnologia actual. Alternativamente, é possível procurar galáxias através das suas características mais brilhantes, as linhas de emissão, o que permite revelar populações de galáxias que não seriam detectadas pela sua emissão no contínuo (e.g. Sobral et al., 2015).

Neste trabalho apresenta-se o maior estudo alguma vez feito para detectar galáxias a redshift $z \sim 6$ utilizando a risca de emissão Lyman-alpha (Lyα, $\lambda = 1215.67$ Å). Esta risca de emissão é desviada para o visível para $z > 2$, tornando-a observável a partir da Terra (outras importantes riscas são absorvidas pela atmosfera terrestre para estes redshifts) o que a torna extremamente útil para estudar o Universo distante. Utilizamos a maior área (e correspondentemente volume) alguma vez utilizada de forma a encontrar fontes mais luminosas (mais raras) que podem muito mais facilmente ser estudadas em detalhe (e.g. Ouchi et al., 2013; Sobral et al., 2015; Hu et al., 2016).

A risca de emissão Lyα está associada a galáxias jovens, com forte formação estelar e a núcleos galácticos activos (AGN), sendo intrinsecamente a risca mais intensa do UV (e.g. Partridge and Peebles, 1967). Devido à sua natureza ressonante, é facilmente absorvida e dispersada por hidrogénio neutro e pode ser usada como ferramenta para testar o estado neutro do meio intergalactico (IGM) durante a época da reionização (e.g. Dijkstra, 2014).

A emissão desta risca em galáxias está associada à presença de estrelas extremamente massivas, de classe espectral O e B. Estas estrelas têm tempos de vida muito curtos e a sua observação indica que existe ou existiu num passado muito próximo um episódio de formação estelar a ocorrer na galáxia. Estas estrelas emitem grandes quantidades de radiação UV altamente ionizante que é absorvida pelo hidrogénio em torno das galáxias e re-emitido como linhas de recombinação, sendo uma das linhas mais comuns a risca de emissão Lyα.

Emissão Lyα em AGNs é originada devido a acreção a altas temperaturas em torno de um buraco negro super massivo. Por alargamento de doppler, riscas de emissão originadas por processos de acreção a alta velocidade são largas (Seyfert, 1943).

Para detectarmos fontes com fortes riscas de emissão utilizamos observações realizadas com filtros de banda estreita (narrow bands) coordenadas com observações com filtros de banda larga (broad bands) para os mesmos comprimentos de onda. Os filtros de banda estreita apenas transmitem radiação numa janela de comprimentos de onda muito pequena e os de banda larga em janelas mais largas. Fontes com forte detecção na banda estreita relativamente à sua detecção na banda larga provavelmente têm um risca de emissão nos comprimentos de onda da banda estreita que contribui para este excesso na detecção. Dois parâmetros, Σ e largura equivalente (equivalent width, EW) são introduzidos para definir o quão significante é o excesso de uma fonte (e.g. Sobral et al., 2013; Matthee et al., 2015).

Para detectar uma fonte com uma risca específica, apenas é necessário determinar o comprimento de onda da risca ao redshift que queremos estudar e construir um filtro de banda estreita em torno desse comprimento de onda. A janela de comprimentos de onda traduz-se numa pequena fatia de redshifts que o filtro consegue analisar, que por sua vez corresponde a um volume.

Diferentes riscas de emissão a diferentes redshifts têm o mesmo comprimento de onda observado. Por isso, para identificar uma risca em específico é necessário aplicar critérios de selecção. Para selecionar emissores Lyα a alto redshift utiliza-se a posição da Lyman Break (e.g. Steidel et al., 1996), ou seja, da "queda" na detecção de radiação para comprimentos de onda mais energéticos que o limite de Lyman a 912 Å, correspondente à energia necessária para ionizar um átomo neutro de hidrogénio.

Utilizamos o filtro NB816 para detectar emissores Lyα a $z = 5.7$ numa área total de 7 graus quadrados (volume de $\sim 10^7$ Mpc^3) nos campos UDS, COSMOS e SA22. Escolhemos estes três campos porque são completamente independentes (prevenindo qualquer influência de estarmos a observar a mesma região do céu) e porque estão bastante afastados do plano da galáxia (evitando forte emissão estelar e poeira). Depois de aplicarmos os critérios de selecção e de cuidadosamente confirmarmos visualmente todas as fontes, obtemos uma amostra de 514 emissores Lyα a $z = 5.7$ e analisamos as suas propriedades.

Realizamos um estudo da variação do tamanho dos emissores com a luminosidade para $z = 5.7$ e $z = 6.6$. Observamos que em média as fontes a $z = 6.6$ são mais extensas, o que é consistente com um período de reionização onde o hidrogénio ainda neutro dispersa a emissão Lyα em halos, consistente com e.g. Momose et al. (2014).

Construímos a função de luminosidade de emissores Lyα a $z = 5.7$, i.e., a distribuição do número de fontes por unidade de volume por luminosidade. Aplicamos uma correcção de completude baseada no fluxo de linha, uma correcção para corrigir a forma do filtro e uma correcção da abertura para converter luminosidades e podermos comparar os nossos resultados com os da literatura.

Obtemos uma função de luminosidade com uma inclinação muito íngreme de $\alpha = -2.3^{+0.4}_{-0.3}$. Fixando $\alpha = -2.0$ medimos $L^\star = 10^{43.22^{+0.08}_{-0.05}}\,\mathrm{erg\,s^{-1}}$ e $\Phi^\star = -3.60^{+0.12}_{-0.16}\,\mathrm{Mpc^{-3}}$. Apresentamos também resultados actualizados de emissores Lyα a $z = 6.6$ de (Matthee et al., 2015).

Estimamos que a variância cósmica representa um papel extremamente importante, com o número de fontes por unidade de volume a variar significativamente dentro da nossa cobertura.

Encontramos evolução significativa entre $z = 5.7$ (depois da reionização) e $z = 6.6$ (dentro da reionização) apenas para as fontes mais ténues. Parece não haver evolução para as fontes mais brilhantes ($L_{Ly\alpha} > 10^{43.5}\,erg\,s^{-1}$), o que é consistente com as fontes mais luminosas ionizarem as suas próprias bolhas de hidrogénio, de dimensões suficientemente grandes para a radiação Lyα escapar.

Os nossos resultados apontam assim para uma época da reionização preferencial que ocorreu primeiro em torno das fontes mais brilhantes.

Palavras-chave: galáxias: alto-redshift – galáxias: função de luminosidade – cosmologia: observações – cosmologia: idade das trevas, reionisação, primeiras estrelas.

Contents

List of Figures

List of Tables

Chapter 1

Introduction

1.1 Universe across cosmic time

Our current view of the Universe has been built over the past century through cosmological models (e.g. Lemaître, 1927; Guth, 1981; Weinberg, 1989), direct observations of the sky (e.g. Hubble, 1929; Penzias and Wilson, 1965; Riess et al., 1998; Perlmutter et al., 1999) and, more recently, with computer simulations (e.g. Klypin and Shandarin, 1983; Springel et al., 2005; Heitmann et al., 2010).

As we stand, we see the Universe as a dynamical and constantly evolving system that is homogeneous and isotropic at the largest scales.

1.1.1 Big Bang Cosmology

The turning point which sparked our current understanding of the Universe was the discovery that galaxies are moving away from us due to the expansion of the Universe. This theory was first proposed by Georges Lemaître (Lemaître, 1927) who applied Einstein's General Relativity to Cosmology and realized that a constantly growing Universe would explain the redshift (increase in wavelength) of emission lines in distant galaxies. Two years later, Edwin Hubble provided the fist observational evidence of the expansion of the Universe by accurately deriving distances to galaxies and comparing them with their receding velocities (Hubble, 1929). Hubble derived a relation of proportionality between the receding velocity (v) of a galaxy and its distance (d) to the observer, know as Hubble's law:

$$v = H_0 d \tag{1.1}$$

Where H_0[1] $= 67.74 \pm 0.46$ km s^{-1} Mpc^{-1} is the Hubble constant.

The redshifting effect which had previously been attributed to a simple Doppler shift caused by the proper movement of galaxies was then interpreted as the expansion of the space itself, with radiation being stretched and its wavelength increased. We can express this shift of radiation to redder wavelengths, redshift (z), as:

$$z = \frac{\lambda_{obs}}{\lambda_{em}} - 1 = \sqrt{\frac{1 + v/c}{1 - v/c}} \tag{1.2}$$

Where λ_{em} is the wavelength of the radiation emitted by a source and λ_{obs} the observed wavelength.

More recently, the expansion of the Universe has been constrained much more accurately using Type Ia Supernovae (e.g. Perlmutter et al., 1999; Kowalski et al., 2008; Amanullah et al., 2010).

A Universe that is expanding must have started somewhere, in some point in the past. This is the line of thought which lead to the development of the Big Bang Cosmology, currently embodied by the ΛCDM ("Lambda Cold Dark Matter") model.

The ΛCDM model is widely regarded as the "standard model" as it provides the most accurate description of the formation and evolution of structure in the Universe and is heavily supported by observational measurements (e.g. observation of the Cosmic Microwave Background, CMB; Penzias and Wilson 1965). This model states the energy density of the Universe is divided into three components: the baryonic matter ($\Omega_b = 0.0486 \pm 0.0010$), the (cold) dark matter ($\Omega_c = 0.2589 \pm 0.0057$) and the dark energy, characterized by the cosmological constant Λ ($\Omega_\Lambda = 0.6911 \pm 0.0062$). Therefore, the baryonic matter, which we can directly observe and interact, only accounts for less than 20% of the matter density parameter $\Omega_m = 0.3089 \pm 0.0062$ and

[1] Historically, the estimates and uncertanties of cosmological parameters significantly changed over the past decades as new instruments and techniques were developed. All the cosmological parameters provided in this section are the latest results from Planck Collaboration et al. (2015) (table 4, last column; revised in June 2016)

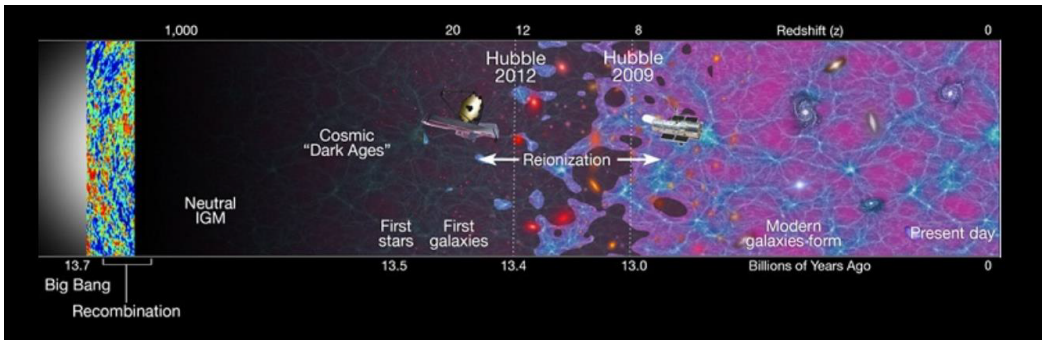

Figure 1.1: Universe across cosmic time according to the Big Bang Cosmology. Starting with the Big Bang and the Recombination, the CMB was emitted the the IGM became neutral. As the Universe expanded and cooled down, first stars and galaxies started forming from primordial density perturbations. The Universe became once again ionized (likely by the first galaxies) during the EoR and entered the "modern ages". Galaxies evolved into our current time, t_0, leaving its evolution imprinted in the SFH of the Universe. Credit: NASA/ESA.

less than 5% of the total energy density of the Universe. This model places the age of the Universe at $t_0 = 1/H_0 = 13.799 \pm 0.021$ Gyr.

1.1.2 Galaxy formation in the early Universe

A simplified timeline of the Universe according to the Big Bang Cosmology is shown in Figure. 1.1.

Following the Big Bang, the Universe was extremely dense and hot, preventing even electromagnetic radiation from escaping due to the highly frequent Thompson scattering by free electrons. As the Universe expanded and cooled down, free electrons and protons bounded and formed neutral atoms of hydrogen in a period of time known as Recombination (Peebles, 1968, $z = 1100,400$ Myrs after the Big Bang). During this time, as a result of photon decoupling from matter, the CMB was emitted. The CMB is widely used to study the early Universe (e.g. Spergel et al., 2003; Dunkley et al., 2009; Komatsu et al., 2009) as it is one of the few direct probes of this epoch.

As the Universe continued to expand, it globally cooled down and processes such as the gravitational collapse of gas became possible. The first structures (such as stars and galaxies) were formed at $z \sim 20 - 50$ (e.g.

Tegmark et al., 1997) by gravitational collapse originated by primordial perturbations in the early Universe. Dark matter wells would trap gas which after cooling down would form stars. The seeds for these perturbations were likely created in a period of rapid expansion right after the Big Bang, the Inflation (Guth, 1981). These density perturbations are observed as fluctuations in the CMB (e.g. Smoot et al., 1992; Bennett et al., 1996; Spergel et al., 2007). The presence of dark matter is thought to have been essential in keeping structures gravitationally bound and, without it, the gravitational collapse of only baryonic matter would have likely been shut down by feedback processes, preventing structures from forming. Even though there is still no clear evidence of a direct detection of dark matter, its existence seems necessary for the formation of structures in the early Universe. Recent observations from the Bullet cluster (1E 0657-56 Markevitch et al., 2002, 2004) also seem to greatly support its existence.

With the first structures being formed, the Universe transitioned into a new period, the Epoch of Reionization (EoR). In this period, the Universe which was neutral after the Recombination was reionized. Results from Planck, place the EoR at $z = 8.8^{+1.2}_{-1.1}$, however, this assumes a step-function instantaneous reionization. Quasar measurements from Fan et al. (2006) clearly show that reionization is still not complete at $z \sim 6$ which points towards a more lasting EoR which was highly inhomogeneous in space and time. Theoretical results from e.g. Cen and Haiman (2000) and observations from e.g. Matthee et al. (2015) and Sobral et al. (2015) support the claim that the EoR occurs in preferred locations, beginning around strong ionizing sources which formed Stromgen spheres (spheres of ionized hydrogen) around them.

It is still uncertain what was responsible for the reionization of the Universe. It was established that quasars alone could not have provided enough ionising photos to reionize the Universe (Willott et al., 2010; Glikman et al., 2011). Robertson et al. (2010) states that galaxies could be responsible for the reionization if the faint end slope of the LF is steeper than -1.6. Recent studies have constrained the ultraviolet (UV) LF from large samples of galaxies at $z \sim 6 - 10$ (e.g. Oesch et al., 2012, 2014; Finkelstein et al., 2015; Bouwens et al., 2015) and measured an extremely steep faint end of

approximately -2 which is consistent with the scenario of galaxies ionizing the Universe with major contribution from the much more abundant faint galaxies. Alternatively, other studies have suggested that bright sources, particularly population III fuelled galaxies, could have had a major role in reionizing the Universe (e.g. Matthee et al., 2015; Sobral et al., 2015).

1.1.3 Star-formation history of the Universe

After the Universe was reionized, the "modern ages" of the Universe began, with galaxies evolving to their current state. To quantify the evolution of these galaxies and how active they were throughout cosmic time, we can measure and compare star-formation rates, i.e, the amount of stars produced per unit of time in an epoch of the Universe. By integrating the star-formation rates of galaxies over volumes, we can obtain star-formation densities (e.g. Sobral et al., 2013).

A galaxy which is actively forming stars leaves several signatures of star-formation that we can take identify. Extremely massive and bright stars, such as O and B, have short life spans of a few million years and their presence indicates that star-formation is happening or has occurred in a very recent past. These stars emit copious amounts of UV radiation which we can observe directly or indirectly. The most common star-formation tracers are: UV radiation that is directly emitted by these stars; emission lines (such as e.g. Hα and [OII]), which are emitted as recombination lines after hydrogen gas around galaxies gets ionized by the highly energetic UV radiation from these stars; far-infrared emission in the form of thermal emission of heated dust; radio emission from supernovae explosions when O and B stars reach the end of their lives.

Using a combination of these tracers, a global picture of the star-formation history (SFH) of the Universe has emerged. After the formation of the first galaxies, the number density of galaxies rose steadily with time, resulting in a steady increase in the star formation density of galaxies until it peaked at $z \sim 2-3$ (~ 10 billion years ago). After that, a decline in the formation of stars has been measured until today. In Figure 1.2 (Khostovan et al., 2015) we show the star-formation density history of the Universe across cosmic time. These results were obtained using emission line selected galaxies (in

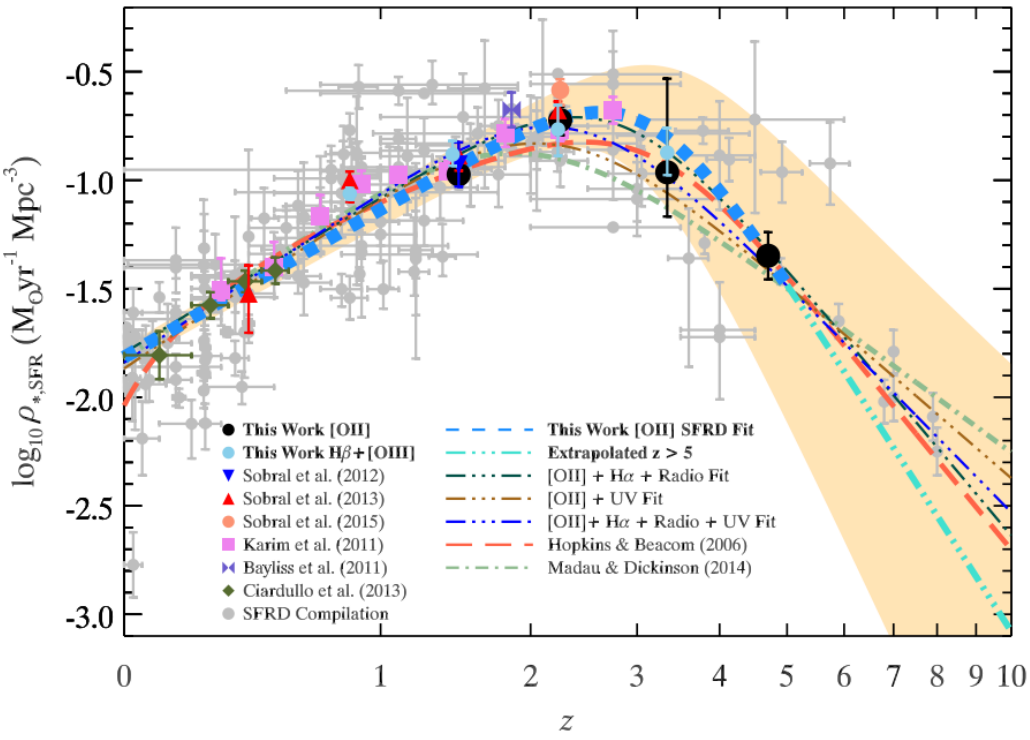

Figure 1.2: Evolution of the star-formation rate density across cosmic time (Khostovan et al., 2015). In this figure the authors present a compilation of measurements from different selection methods. The highlighted points were determined from emission line selected galaxies (in this case Hβ+[OIII] and [OII]) using the same technique. This emphasizes the accuracy that can be achieved from consistently using the same approach (as opposed to comparing completely different samples; greyed out points). Results from different methods (including UV, IR and radio) seem to agree that galaxies formed more stars at $z \sim 2-3$ and the star-formation rate density continuously decreased both for higher and lower redshifts.

this case Hβ+[OIII] and [OII]) which are overall consistent with results from UV, infra-red (IR) and Radio. It should be noted that the highlighted points from the plot, which were obtained with the same technique, constrain much more accurately the star-formation density history.

1.2 High redshift searches

Observations of the high-redshift Universe allow us to directly peak at the first galaxies and stars. These observations provide us with constrains on cosmological models and simulations and are essential to get the most accurate measurements of the cosmological parameters.

During the past two decades, considerable progress has been made in directly observing the distant/early Universe (see reviews by e.g. Robertson et al., 2010; Dunlop et al., 2012; Madau and Dickinson, 2014). Currently, the samples of $z > 6$ candidates are mostly composed by rest-frame UV selected galaxies obtained from extremely deep surveys with the Hubble Space Telescope (e.g. Bouwens et al., 2015; Finkelstein et al., 2015). However, spectroscopy and multi-wavelength follow-up (e.g. with ALMA; Ouchi et al., 2013; Watson et al., 2015; Capak et al., 2015; Maiolino et al., 2015) of these sources still remains very limited as most candidates are too faint for a detailed analysis with current instrumentation (see also Dunlop et al., 2016).

Alternatively, emission lines can be used to search for high-redshift galaxies to directly select galaxies by their brightest features, including several rest-frame optical and UV lines (e.g. Ouchi et al., 2008; Sobral et al., 2013; Khostovan et al., 2015, 2016), allowing for efficient follow-up strategies.

1.3 The Lyman-α emission line

The Lyman-α (Lyα)[2] emission line (rest-frame 1215.67 Å) is a recombination line associated with both young star-forming galaxies and active galactic nuclei(AGN)/quasars, being intrinsically the strongest emission line in the rest-frame optical to UV (e.g. Partridge and Peebles, 1967; Pritchet, 1994).

[2] see Appendix A for a more detailed explanation of the Lyman series from the hydrogen atom

As Lyα is redshifted into optical wavelengths (it can be observed from the ground at $z \approx 2 - 7$), many other strong lines are redshifted out of even the near-infrared (see e.g. Ly et al., 2007, 2011; Hayes et al., 2010; Sobral et al., 2013), making Lyα one of the only available means of spectroscopic confirmation, along with other weaker high ionisation UV lines (e.g. Sobral et al., 2015; Stark et al., 2016).

As detailed in section 1.1.3, massive stars such as O and B are present in galaxies which are going through star-formation periods. These stars emit highly energetic UV radiation which gets absorbed by the hydrogen in the IGM and re-emitted in the form of emission lines, such as Lyα. Lyα is intrinsically a star-formation tracer (Nilsson et al., 2007) as it is one the most prominent recombination lines, however, due to its complex resonant nature and because it gets easily absorbed and scattered, it is extremely challenging to derive star-formation rates from this line. Combined Hα-Lyα surveys (Hayes et al., 2011; Matthee et al., 2016b) can shed some light on what affects the observability of Lyα, such as the escape fraction.

Lyα emission in quasars and AGNs is originated from strong UV emission from heated accretion disks around massive black holes which can create Lyα haloes (e.g. Charlot and Fall, 1993; Weidinger et al., 2005). High speed accretion creates broad emission lines due to Doppler shifts (e.g. Seyfert, 1943).

1.3.1 Lyα as a probe of reionization

Due to its resonant nature, Lyα photons are easily scattered by neutral hydrogen (and also easily absorbed by dust; e.g. Hayes et al., 2011). As a consequence, the observability of Lyα can in principle be used as a probe of the neutral state of the inter-galactic medium (IGM) during the epoch of reionization (e.g. Dijkstra, 2014; Pentericci et al., 2014; Schmidt et al., 2016). However, in order to interpret Lyα observations (such as the distribution of equivalent widths, the fraction of UV selected galaxies with strong Lyα, or the evolution of the number density of Lyα emitters) as consequences of reionization, one needs to accurately understand the contribution from potentially varying intrinsic inter-stellar medium (ISM) properties such as the Lyα escape fraction (c.f. Matthee et al., 2016b) or selection biases in UV se-

lected galaxy samples (c.f. Oesch et al., 2015; Zitrin et al., 2015; Stark et al., 2016).

Therefore, it is important to have a clear understanding of Lyα with only little influence from the IGM at $z \approx 6$, when reionization is close to complete and the fraction of neutral hydrogen becomes extremely low (Fan et al., 2006; Becker et al., 2015).

1.3.2 Searches for Lyα emitters

Several approaches have been used to find and study Lyα emitters, including blind spectroscopy (e.g. Martin and Sawicki, 2004; Stark et al., 2007; Rauch et al., 2008; Sawicki et al., 2008; Bayliss et al., 2010; Cassata et al., 2011), narrow band surveys (e.g. Cowie and Hu, 1998; Rhoads et al., 2000, 2003; Malhotra and Rhoads, 2004; Taniguchi et al., 2005; Shimasaku et al., 2006; Westra et al., 2006; Iye et al., 2006; Nilsson et al., 2007; Murayama et al., 2007; Ouchi et al., 2008, 2010; Sobral et al., 2009; Hu et al., 2010; Kashikawa et al., 2011; Shibuya et al., 2012; Konno et al., 2014; Matthee et al., 2014, 2015) and Integral Field Unit (IFU) observations (e.g. Blanc et al., 2011; Adams et al., 2011; van Breukelen et al., 2005; Bacon et al., 2015; Karman et al., 2015).

Blind spectroscopy and IFU surveys can be very efficient at probing ultra-low luminosity sources at a variety of redshifts, but the current small volumes probed make them unable to reach even L^* sources, as the rarer (brighter) sources have number densities several times smaller that these studies can reach.

Wide narrow band surveys can be very competitive at efficiently probing large volumes at specific look-back times, and can be used to study a much larger luminosity range. For example, one MUSE pointing (e.g. Bacon et al., 2015) probes a volume of $\sim 10^3\,\mathrm{Mpc}^3$ for $z \sim 3-6$, while one Subaru Suprime-Cam pointing with a typical narrow band filter probes a volume of $\sim 10^5$ Mpc^3 (Hyper Suprime-Cam covers a volume ~ 7 times larger per pointing). Typically, narrow band surveys have targeted a maximum of $\sim 1\,\mathrm{deg}^2$ areas, corresponding to maximum volumes of $\sim 10^6$ Mpc^3 (e.g. Ouchi et al., 2008, 2010), but the next generation of surveys are now starting to probe much larger volumes (e.g. Matthee et al., 2015; Hu et al., 2016).

1.3.3 Evolution of the Lyα luminosity function

The luminosity function (LF) is one of the most important probes of the early Universe, consisting on the number density distribution of galaxies as a function of their luminosity.

Previous studies found that the Lyα LF seems to have little evolution at $z \sim 3-6$ (e.g. Ouchi et al., 2008, Figure 1.3, right). In contrast, the UV LF of Lyman-break galaxies (LBGs) strongly decreases for higher redshifts (e.g. Bouwens et al., 2015; Finkelstein et al., 2015, Figure 1.3, left). This difference in evolution is likely explained by an evolving escape fraction of Lyα photons, likely due to a lower dust content, younger stellar populations, lower metallicities and/or a combination of related phenomena. This is consistent with the observation that the fraction of LBGs with strong Lyα emission increases up to $z = 6$ (e.g. Stark et al., 2010; Cassata et al., 2015).

At $z > 6$ the number density of faint Lyα emitters (LAEs) is found to decline with redshift (Ouchi et al., 2010; Konno et al., 2014), likely due to reionization not being fully completed. However, by using the largest Lyα survey at $z \sim 7$ ($\sim 5\,\mathrm{deg}^2$), Matthee et al. (2015) shows that the strong decrease/evolution in the number density of LAEs happens pre-dominantly at relative faint Lyα luminosities, while the bright end (with luminosities $\mathrm{L}_{\mathrm{Ly}\alpha} > 10^{43}\,\mathrm{erg\,s^{-1}}$) may not evolve at all. Matthee et al. (2015) finds that bright LAEs at $z = 6.6$ are much more common than previously thought, with spectroscopic confirmation presented in Sobral et al. (2015), and with independent studies finding consistent results (see e.g. Hu et al., 2016). However, one strong limitation in interpreting the potential evolution from $z = 6.6$ to $z = 5.7$ is the lack of comparably large $\sim 5-10\,\mathrm{deg}^2$, multiple field surveys that can both trace a large enough number of bright sources and overcome cosmic variance. We will be addressing this limitation by providing a comparable survey at $z \sim 6$.

1.4 This study

In this work, we present the largest Lyα narrow band survey at $z = 5.7$, covering a total of $\sim 7\,\mathrm{deg}^2$ ($\sim 10^7\,\mathrm{Mpc}^3$). Previous studies have never probed beyond $2\,\mathrm{deg}^2$ (e.g. Murayama et al., 2007; Ouchi et al., 2008; Hu

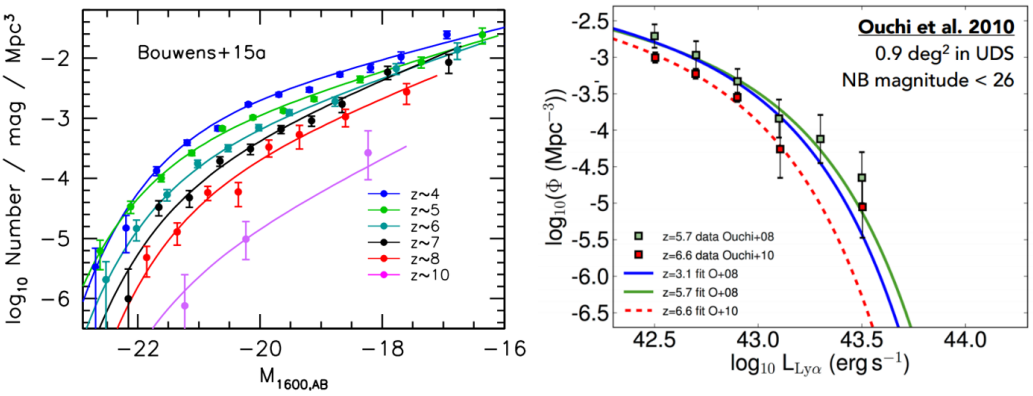

Figure 1.3: Collection of LFs from UV-selected galaxies (Bouwens et al., 2015, left) and Lyα-selected galaxies (Ouchi et al., 2008, right). For the UV-selected LBGs there is a clear drop in the LF for higher redshifts. This can likely be explained by a decrease in the SFH as we go to higher redshifts (e.g. Khostovan et al., 2015, Figure 1.2). In contrast, the Lyα LF seems to have little to no evolution at $z \sim 3-6$. The differences we observe in the Lyα LF evolution may be explained by an evolving escape fraction of Lyα photons, associated with the complex nature of Lyα emission.

et al., 2010), and have mostly focused on specific, single fields. Here we take advantage of previous data and add further $\sim 4\,\mathrm{deg}^2$ of unexplored data. We also re-analyse the $z = 6.6$ luminosity function presented in Matthee et al. (2015).

We structure this dissertation as follows: Chapter 2 explains the methodology applied in narrow band searches for line-emitters. Chapter 3.1 presents the observations and data reduction. Chapter 4.1 explains the selection of line-emitters and Lyα emitters at $z = 5.7$. In Chapter 5 we present the method and procedures adopted to construct the $z = 5.7$ and $z = 6.6$ Lyα LFs. We present our results in Chapter 6, including a comparison with previous surveys. Chapter 7 discusses the results in the context of predicted effects from reionization. Finally Chapter 8 presents the conclusions of this dissertation.

Throughout this work, for simplicity and comparability with other studies, we use a "737" ΛCDM cosmology with $\mathrm{H}_0 = 70\,\mathrm{km\,s^{-1}\,Mpc^{-1}}$, $\Omega_M = 0.3$ and $\Omega_\Lambda = 0.7$. This is a close estimate to the Planck Collaboration et al. (2015) measurements provided in section 1.1.

All magnitudes in this dissertation are presented in the AB system. At $z = 5.7$, $1''$ corresponds to 5.9 kpc.

Chapter 2

Methodology

As previously stated, several approaches have been used to probe distant sources with strong line-emission (e.g. blind spectroscopy, IFU observations and narrow band surveys). In this chapter we will focus on the methodology we follow to conduct our narrow band survey to select high-redshift galaxies with strong Lyα emission.

2.1 Narrow Band Technique

A narrow band survey consists on the imaging of a region of the sky using a narrow band filter, i.e., a filter that only transmits radiation inside a narrow window of wavelengths, typically in a small range of ~ 100 Å (broad band filters cover much larger widths, usually an order of magnitude larger than narrow bands, e.g. Capak et al., 2007). In Figure 2.1 we show a collection of narrow band filters currently available in ground-based telescopes such as the Subaru Telescope, the Isaac Newton Telescope (INT) and the Canada-France-Hawaii Telescope (CFHT). Narrow band filters are built to probe ranges of wavelengths with low atmospheric emission from OH molecules, making ground-based photometry extremely reliable and detected sources well suitable for detailed follow-up observations (e.g. Ouchi et al., 2013; Sobral et al., 2015; Hu et al., 2016).

Observations of the sky with a narrow band filter can be used to unveil specific features of sources such as emission lines. We can identify sources with strong line-emission by comparing narrow band and broad band detections at similar wavelengths. Any source with a strong narrow band detection

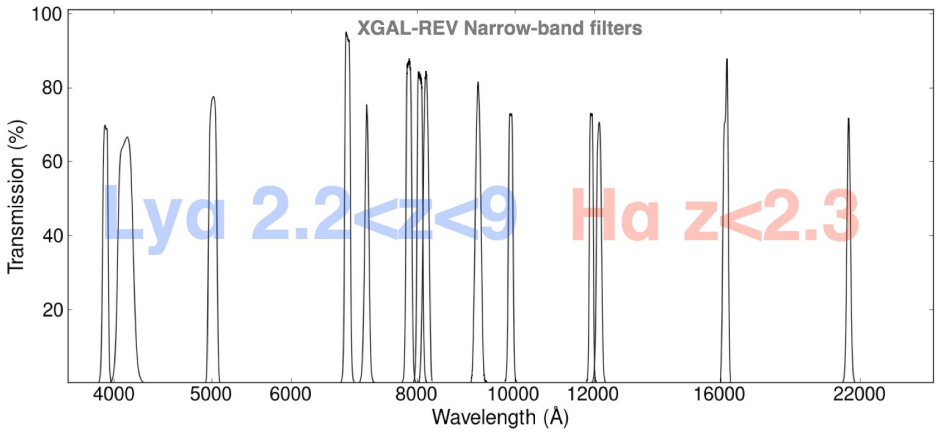

Figure 2.1: A summary of the full set of narrow-band filters available for use in the INT, Subaru and CFHT. All the filters are built in wavelength windows with no atmospheric emission, making ground-based photometry extremely reliable. These narrow bands provide a set of redshift slices that allow us to probe the Universe starting locally and all the way up to $z \sim 9$. Line-emitters are selected by the Hα emission line up to $z = 2.2$ and with Lyα for higher redshifts. There is a small window at $z = 2.2$ where both lines can be observed, giving the opportunity for Hα-Lyα combined surveys.

relatively to its broad band counterpart likely has an emission line inside the narrow band coverage which is boosting its detection. For visual reference we show in Figure 2.3 a fiducial source with a strong emission line (template from photometric redshift code EAZY, Brammer et al., 2008) with a narrow band and a broad band placed around its central wavelength. The broad band, which is much wider than the emission line, gives an estimate on the continuum emission while the small width of the narrow band filter mostly probes the emission line.

To exemplify the narrow band selection technique we show in Figure 2.2 three panels of a line-emitter (in this case with strong Hα emission) from (Sobral et al., 2012). From left to right we present the broad band imaging, the narrow band imaging and the excess imaging. The excess image is obtained by subtracting the first two images and highlights sources with high narrow band excess (broad band magnitude minus narrow band magnitude, $BB - NB$), i.e. sources with strong emission in the narrow band image relatively to its broad band counterpart. The line-emitters we are searching for

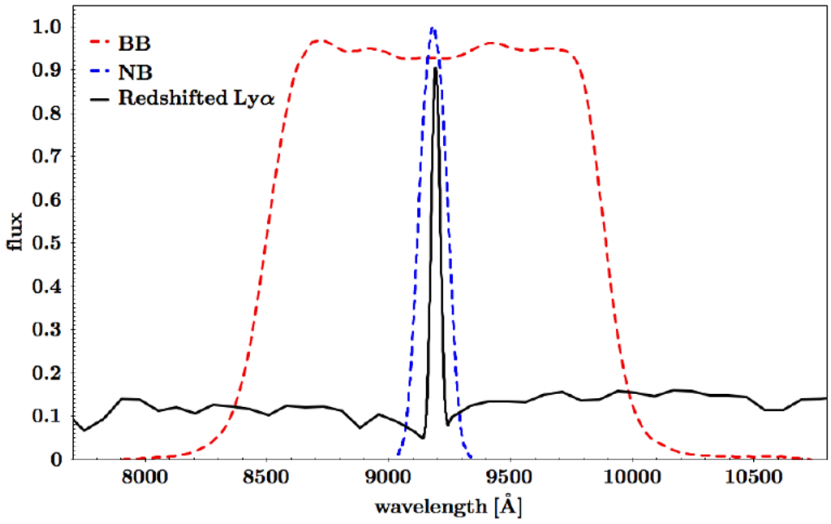

Figure 2.2: Fiducial emission line (created from a template from the photometric redshift code EAZY, Brammer et al., 2008) with one narrow band filter and one broad band filter built around its central wavelength. The narrow band filter probes mostly the emission line while the broad band gives an estimate on the continuum emission.

in our survey are thus sources which are bright in the narrow band images but may not even be detected in the broad bands.

It is important to establish what defines a line-emitter. How high does the narrow band excess of a source needs to be for it to be classified as a line-emitter? We need to define parameters that quantify what is the significance of an excess. These parameters need to be dependent not only on the measured photometry but also on uncertainties introduced by observations, such as the background noise of the imaging. So, for the selection of line-emitters, we apply similar criteria to e.g. Sobral et al. (2013) and Matthee et al. (2015), relying on two parameters: equivalent width (EW) and Sigma (Σ).

2.1.1 Σ parameter

To define if a source is a line-emitter, we start by establishing how significantly above the background noise the narrow band excess of that source is.

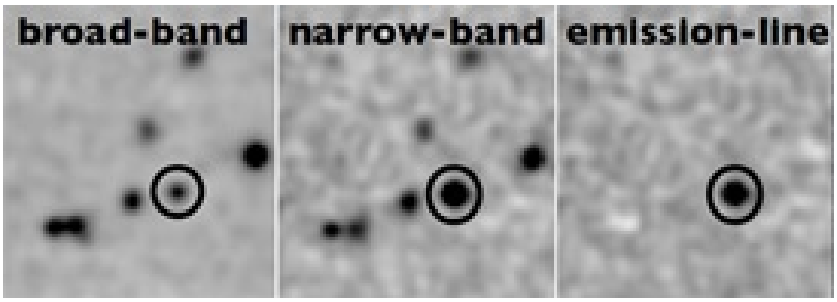

Figure 2.3: Hα line-emitter Sobral et al. (2012) that illustrates the narrow band selection. (From right to left) Broad band image, narrow band image and excess image. The excess image is obtained by subtracting the broad band to the narrow band. Sources with high narrow band excess (line-emitters) become clearly visible.

As a first order approximation, we can consider there is no background noise in the images and all the counts come from our source. In this simple scenario, any source which agrees with the follow equation would be considered a line-emitter:

$$\text{counts}_{NB} - \text{counts}_{BB} > 0 \tag{2.1}$$

Where counts_{NB} and counts_{BB} are the counts in ADUs [1] from the narrow band and broad band images, respectively.

However, since we cannot neglect the uncertainties introduced by the background of the images, we need to introduce the parameter Σ (e.g. Bunker et al., 1995) that assures the excess of the narrow band relative to the broad band is significantly above the noise. The difference between the counts needs to be bigger than the root sum square of the background noise from both images scaled by their significance Σ. Equation 2.1 can thus be generalized as:

$$\text{counts}_{NB} - \text{counts}_{BB} > \Sigma \times \sqrt{rms_{NB}^2 - rms_{BB}^2} \tag{2.2}$$

Where rms is the root-mean-square of the background of the respective

[1] Analog/Digital Unit, the standard unit of measure for the values in a CCD imaging obtained from the number of electrons collected weighted by the collection efficiency of the CCD

image (we measure the rms with randomly placed 2" apertures, further detailed in section 3.2).

We proceed to convert counts into magnitudes:

$$\text{magnitude} = \text{-2.5 } \log_{10}\text{counts} + \text{ZP} \tag{2.3}$$

Where ZP is the zero point of an image - a value that is used to calibrate magnitudes and corresponds to the magnitude of a source that produces 1 count (per unit of time), which cancels the logarithmic term of the equation.

Therefore, we can write Σ as (Sobral et al., 2013):

$$\Sigma = \frac{1 - 10^{-0.4(BB-NB)}}{10^{-0.4(ZP-NB)}\sqrt{rms_{BB}^2 + rms_{NB}^2}} \tag{2.4}$$

Where BB and NB are the magnitudes in the broad band and narrow band images, respectively.

2.1.2 Equivalent Width

An additional parameter is added to define how strong a line is - the equivalent width (EW) (e.g. Bunker et al., 1995). The EW is the ratio between the flux of an emission line and the continuum flux, meaning that higher narrow band excess translates into higher EWs. It can be expressed as:

$$EW_{obs} = \Delta\lambda_{NB}\frac{f_{NB} - f_{BB}}{f_{BB} - f_{NB}(\Delta\lambda_{NB}/\Delta\lambda_{BB})}, \tag{2.5}$$

Where EW_{obs} is the observed EW, $\Delta\lambda_{NB}$ and $\Delta\lambda_{BB}$ are the FWHM (full width at half maximum) of the narrow band and broad band filters and f_{NB} and f_{BB} are the flux densities measured in the two filters.

The flux-density (f) of a source can be expressed as (ZP set to 30):

$$f = \frac{c}{\lambda_c^2}10^{-0.4(m+48.6)} \tag{2.6}$$

Where c is the speed of light, λ_c is the central wavelength of the filter and m is the magnitude of the source from the imaging of the same filter.

It should be noted that the observed EW increases with redshift (z), with the rest-frame EW (EW_0) being given by:

$$EW_0 = \frac{EW_{obs}}{1+z} \tag{2.7}$$

For our high-z line-emitter search, we will thus be selecting sources with higher observed EWs (the values for the EW selection are discussed in section 4.1).

2.1.3 Redshifted emission lines

As the redshift of a source increases, the entire spectrum is shifted to redder wavelengths, with some lines moving all the way from rest-frame UV to observed near-infrared (NIR) (e.g. Lyα at $z \gtrsim 5$). This effect plays a major role on what is detected by the narrow band filter and which line (if any) falls inside its small coverage.

The observed wavelength ($\lambda_{\rm obs}$) can be expressed in terms of rest-frame wavelength (λ_0) and the redshift (z) of the source which is emitting the radiation:

$$\lambda_{\rm obs} = \lambda_0(1+z) \tag{2.8}$$

Narrow band surveys have relied on several different emission lines to select line-emitters and probe a large range of redshifts. Some of the most prominent lines are, for example: Hα ($\lambda = 6563$ Å) (e.g. Ly et al., 2007, 2011; Hayes et al., 2010; Sobral et al., 2013), Hβ ($\lambda = 4861$ Å) in combination with the dublet [OIII] ($\lambda = 4959, 5007$ Å) (e.g. Khostovan et al., 2015, 2016), [OII] ($\lambda = 3727$ Å) (e.g. Takahashi et al., 2007; Sobral et al., 2012; Hayashi et al., 2013) and Lyα ($\lambda = 1216$ Å) (e.g. Murayama et al., 2007; Ouchi et al., 2008; Hu et al., 2010). From ground-based telescopes, Hα can be observed at $z \lesssim 2$, Hβ+[OIII] at $z \lesssim 3$, [OII] at $z \sim 1-5$ and Lyα at $z \sim 2-7$. Lyα is the only strong emission line we can use to study $z \sim 5-7$, aside from much weaker high ionising UV lines like CIII] ($\lambda = 1907, 1909$ Å) (e.g. Stark et al., 2016) and HeII ($\lambda = 1640$ Å) (e.g. Sobral et al., 2015).

At $z \sim 5-7$, Lyα gets redshifted into ~ 9000 Å (NIR). Custom narrow band filters were built to select LAEs around this redshift range: NB816 ($\lambda_c = 8150$ Å), NB912 ($\lambda_c = 9140$ Å) and NB921 ($\lambda_c = 9210$ Å). Each filter, due to its small window of coverage, detects Lyα emission from galaxies in a narrow redshift slice, corresponding (for these three filters) to approximately $z \sim 5.65-5.75$, $z \sim 6.45-6.55$ and $z \sim 6.52-6.62$, respectively. The small redshift slices translate into small commoving volumes per unit of area

observed. However, the large areas typically probed by narrow band surveys (~ 1 deg^2) translate into large volumes ($\sim 10^6$ Mpc^3) which greatly surpass most high-z surveys (e.g. MUSE searches for $z \sim 3-6$ LAEs in an area of 1 arcmin^2 and a volume of $\sim 10^3$ Mpc^3 per pointing; HST WFC3 has a small field-of-view (FOV) of ~ 5 arcmin^2). Narrow band surveys are clearly more efficient at probing large volumes. Hundreds of pointings would be required to make other approaches competitive in terms of volume versus already existent narrow band surveys.

Selecting a sample of galaxies in small redshift slices allows us to very accurately study specific time scales. When used in combination with other narrow band surveys at different redshift slices, it provides a well defined view on how properties (e.g. star formation rate) change within each population and establish how they evolve across cosmic time. The comparison between samples becomes easier as all sources are selected on wavelengths free of OH atmospheric lines (a significant portion of the $z \sim 3-6$ volume in MUSE searches is lost due to atmospheric emission).

Due to the redshifting effect, different emission lines have the same observed wavelength at different redshifts. One narrow band can detect several lines, each at a specific redshift window. For example, the narrow band NB921 (shown in Figure 2.3), centered at 9210 Å is sensible not only to Lyα emission at $z = 6.6$ but also to Hα at $z = 0.40$, Hβ+[OIII] at $z = 0.83$ and [OII] at $z = 1.46$. The narrow band selection technique selects sources with strong line-emission inside the narrow band coverage, however, it does not distinguish which line is causing the excess in the narrow band photometry. Additional techniques are thus required to identify the redshift of the different populations of line-emitters (detailed discussion in section 2.2).

2.1.4 Width and shape of narrow band filters

As previously stated, typical narrow band filters have FWHM of ~ 100 Å. Some filters are slightly broader or narrower. For example, the narrow-band filter NB392 ($\lambda_c = 3918$ Å; sensitive to Lyα emission at $z = 2.22$) has a FWHM of 52 Å while medium-bands from e.g. SHARDS (Survey for High-z Absorption Red and Dead Sources, Pérez-González et al., 2013) have typical FWHM of ~ 170 Å. The narrower a filter the deeper it can observe as less sky

background is measured and we get a better S/N ratio for our line-emitters. However, we do this at the cost of probing less volume as a smaller redshift slice translates into smaller commoving volumes. Broader filters will thus probe larger volumes for the same area but will be less deep as they detect much more continuum emission from the line-emitter as well as much more sky background.

A compromise between measured S/N and probed volume is thus taken when defining the width of a narrow band filter.

It is important to note that the transmission of a narrow band filter is not top-hat and changes with wavelength. The filters typically have a gaussian-like shape (e.g. 2.2) which means the filter transmission is lower in the borders and emission lines will be detected at a fraction of their flux unless they are centered with the filter. An example of a source detected at a fraction of its flux is the spectroscopically confirmed $z = 6.604$ galaxy CR7 (COSMOS redshift 7 Matthee et al., 2015; Sobral et al., 2015) which is only detected at $\sim 50\%$ transmission by the narrow band NB921, i.e., NB921 only captures $\sim 50\%$ of the observed Lyα flux. We apply a correction when constructing our luminosity function in section 5.2 so that we don't underestimated the luminosities of our sample.

2.1.5 Overview

In order to identify populations of line-emitters with the narrow band selection technique, we simply need to coordinate narrow band and broad band observations at similar wavelengths. As it only requires imaging observations with two filters, narrow band surveys are extremely efficient at probing large regions of the sky without consuming much telescope time. Observations can be conducted by telescopes/instruments with large FOV such as, for example, the VISTA (Visible and Infrared Survey Telescope for Astronomy) VIRCAM (VISTA InfraRed CAMera), the Suprime-Cam (Subaru Prime Focus Camera) which was recently replaced by the Hyper Suprime-Cam in the Subaru Telescope or the smaller 2.5 meter INT using the WFC (Wide Field Camera). In this study, we use observations with the narrow band filter NB816 (Subaru/Suprime-cam) and the broad band filter i (Subaru/Suprime-cam and CFHT/MegaCam) (see Figure 3.1 for the profiles of these two filters;

further information about the observations is presented in section 3.1). These two filters allow us to select $z = 5.7$ LAEs.

The small redshift slices probed by the narrow bands translate into small commoving volumes per unit of area, however, the wide areas observed by the wide field cameras allow us to surpass most broad band surveys in terms of probed volume.

Selecting sources by their high narrow band excess is selecting sources by their brightest features in a way that optimizes the S/N ratio of the lines (reduced background emission due to the narrow transmission window). Emission lines can be several times brighter than continuum emission and even extremely deep broad band surveys may completely miss them as they probe the much fainter continuum. An example of this selection is the spectroscopically confirmed $z = 6.541$ galaxy MASOSA[2] (Matthee et al., 2015; Sobral et al., 2015) which has a booming detection in the narrow band NB921 (mag=23.84) but is completely undetected by all broad bands except for an extremely faint detection (mag=26.28) in the broad band z' (likely explained by the continuum photometry being boosted by the Lyα emission line) (we show the thumbnails of this source in Figure 2.5). The photometry of this source also provides some extremely interesting implications: strong LAEs are not necessarily UV bright galaxies. This implies that results from typical UV searches may not hold for our Lyα selected sample of galaxies.

One of the main concerns with the narrow band technique that should be carefully tackled is that fake sources such as cosmic rays and spurious sources from dithering patterns detected in the narrow band can be easily mistaken as line-emitters (moving sources can also lead to false positives; further discussed in section 5.5). These fake sources will have strong narrow band excess as they will be detected in the narrow band imaging but will have no detection in the corresponding broad band. Most of these wrongly classified line-emitters should be removed through stacking off several dithered frames as fake emitters will not be detected in the same position in every frame. We apply further criteria to ensure the authenticity of a source, based on their narrow band excess (section 3.4.2), measurement of the standard deviation

[2]the nickname MASOSA consists of the initials of the first three authors: Matthee, Sobral and Santos

to remove cosmic rays (section 3.4.3) and through careful visual checks.

As a narrow band survey can be sensible to several different emission lines at different redshifts, narrow band surveys require additional follow-up techniques in order to isolate samples from each line. We will be discussing those selection procedures in the following section.

2.2 Lyman Break Technique

In this section we present the Lyman Break Technique (Steidel et al., 1996) as a method to select high-z galaxies by using the position of the Lyman limit[3] break at rest-frame 912 Å in combination with the Gunn–Peterson trough effect to establish the redshift of a source.

Radiation more energetic than the Lyman limit gets easily absorbed and scattered by the neutral hydrogen around galaxies (and is usually re-emitted as recombination lines). A significant break can be seen in the spectra of galaxies as radiation blueward of rest-frame 912 Å does not reach the observer but redder radiation does. The position of this break indicates the redshift of the source, as seen by the spectral energy distribution (SED) of $z \sim 6$ quasars in Figure 2.4 (Fan et al., 2006).

2.2.1 Gunn–Peterson trough

An extension of the mentioned break from the Lyman limit to the Lyα line for $z \gtrsim 6$ was proposed by Gunn and Peterson (1965) and first observed by Becker et al. (2001). Neutral hydrogen absorbs radiation blueward of the Lyα line 1216 Å. Radiation which passes through patches of neutral hydrogen will have a break at 1216 Å (rest-frame of the patch). As radiation is redshifted this will create several drops between 912 Å and 1216 Å, known as the Lyman forest. If reionization is still not completed around a source all the radiation blueward of Lyα will be entirely absorbed/scattered by the neutral hydrogen.

With the two effects combined we expect no rest-frame UV (observed optical) detections. As an example, we show thumbnails of two Lyα-selected spec-

[3] see Appendix A for a more detailed explanation of the Lyman series from the hydrogen atom

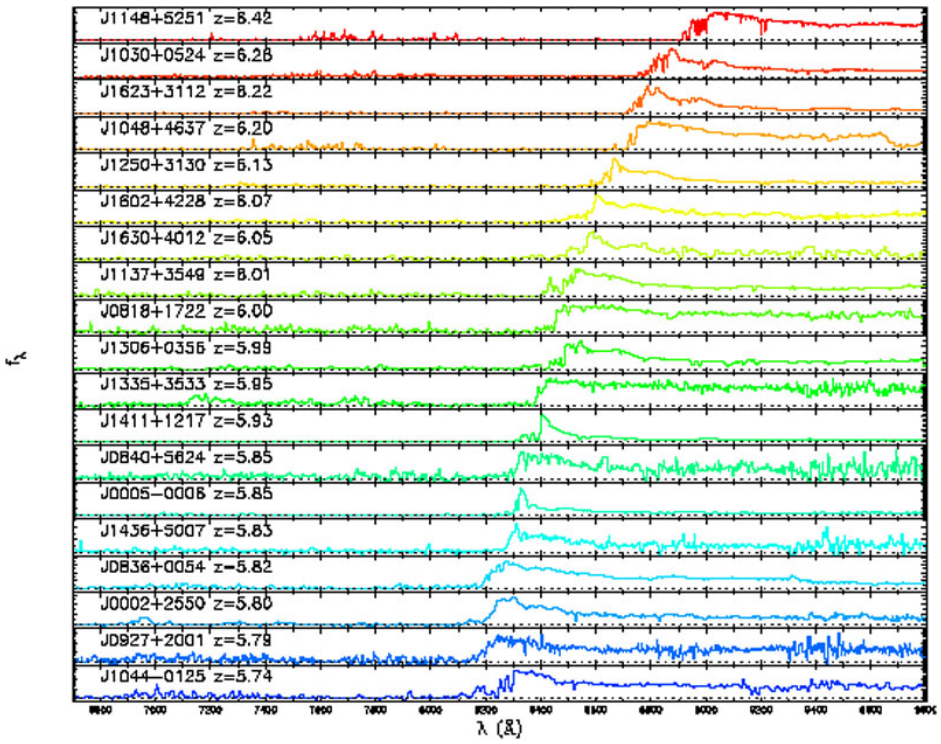

Figure 2.4: Spectral energy distribution of 19 $z \sim 6$ quasars from (Fan et al., 2006). The position of the Lyman break indicates the redshift of the source. For the lower redshift quasars a more accentuated Lyman forest is visible, which clearly disappears for the higher redshift sources.

troscopically confirmed $z = 6.6$ sources which demonstrate this behaviour in Figure 2.5.

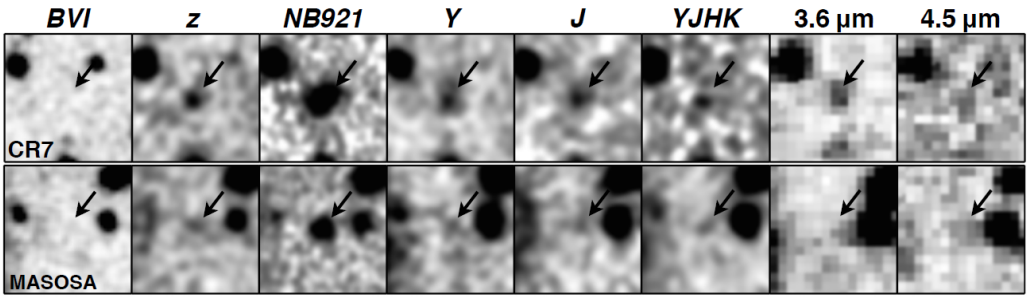

Figure 2.5: Thumbnails from two $z = 6.6$ spectroscopically confirmed galaxies: CR7 (top) and MASOSA (bottom) (Sobral et al., 2015). From left to right we show the BVI optical stack (sources not detected), the broad band z, the narrow band NB921 (which is contained inside z), the NIR bands Y and J (including the YJHK NIR stack) and the two IRAC bands 3.6 μm and 4.5 μm.

Chapter 3

Data

3.1 Observations

We have reduced and analyzed raw archival NB816 data in the COSMOS, UDS and SA22 fields. We use these three fields as they are completely independent (preventing any possible bias from probing the same region of the sky) and far enough from the galactic plane (avoiding bright foreground stars and dust). Additionally, the available deep multi-wavelength coverage (including optical and near infra-red) allows a robust selection of candidates and identification of any lower redshift interlopers.

The NB816 filter has a central wavelength of 8150 Å and a full width at half maximum (FWHM) of 120 Å. NB816 is contained within the red wing of the broad band filter i (see Figure 3.1). All NB816 data were collected with the Suprime-Cam instrument from the Subaru Telescope (Miyazaki et al., 2002). Suprime-Cam has ten 2048x4096 CCDs arranged in a 5×2 pattern, with a corresponding field of view of $\sim 0.25\,\mathrm{deg}^2$. We use a total of 30 of these pointings. Suprime-cam images have a pixel scale of $0.20''\,\mathrm{pix}^{-1}$.

We retrieved all publicly available raw NB816 data for the UDS and SA22 fields from the SMOKA Archive[1]. Fully reduced COSMOS NB816 images (original PSF) were retrieved from the COSMOS Archive[2] (Taniguchi et al., 2007; Capak et al., 2007).

We split SA22 data into two different sub-fields (SA22-deep and SA22-wide), which differ in depth by ≈ 1 mag and in area by a factor of ≈ 6.6.

[1] http://smoka.nao.ac.jp/
[2] http://irsa.ipac.caltech.edu/data/COSMOS/

Table 3.1: Our NB816 data in the COSMOS, UDS and SA22 fields. The SA22 field was separated into two sub-fields, deep and wide, according to its significantly different NB816 depth. R.A. and Dec. are the central coordinates of the fields. FWHM is the average value for the seeing and is similar across our entire coverage. The NB816 depth is the 2σ depth measured in $2''$ apertures. Note that the quoted area already takes into account the removed/masked regions which are not used in this dissertation.

Field	**R.A.** (J2000)	**Dec.** (J2000)	**Area** (deg^2)	**FWHM** ($''$)	**NB816 depth** (2σ, $2''$)
COSMOS	10 00 00	+02 10 00	2.00	0.7	26.2
UDS	02 18 00	−05 00 00	0.85	0.7	26.1
SA22-deep	22 18 00	+00 20 00	0.55	0.7	26.1
SA22-wide	22 15 00	+00 50 00	3.60	0.5	25.0

SA22-wide contains the largest area (larger than COSMOS and UDS combined). Narrow band observations are summarized in Table 3.1.

Previous studies have separately used NB816 data in COSMOS (Murayama et al., 2007), UDS/SXDF (Ouchi et al., 2008) and SA22-deep (~ 0.4 deg^2; Hu et al., 2010). We note that while we explore new data and provide the largest survey of its kind, we are able to reproduce individual results from the literature using our own analysis. A comparison between our findings and previous studies is presented in Section 5.

3.2 Data reduction

We used the Subaru data reduction pipelines (SFRED and SFRED2; Ouchi et al., 2004) to reduce the NB816 data. The data reduction follows the same procedure as detailed in e.g. Matthee et al. (2015) and we refer the reader to that study for more details. Briefly, the reduction steps include: overscan and bias subtraction, flat fielding, point spread function homogenisation, sky background subtraction and bad pixel masking. After these steps, we apply an astrometric calibration using SCAMP (Bertin, 2006) to correct astrometric distortions. The software matches our images with the 2MASS catalog in the J band (Skrutskie et al., 2006) and fits polynomial functions that correct for

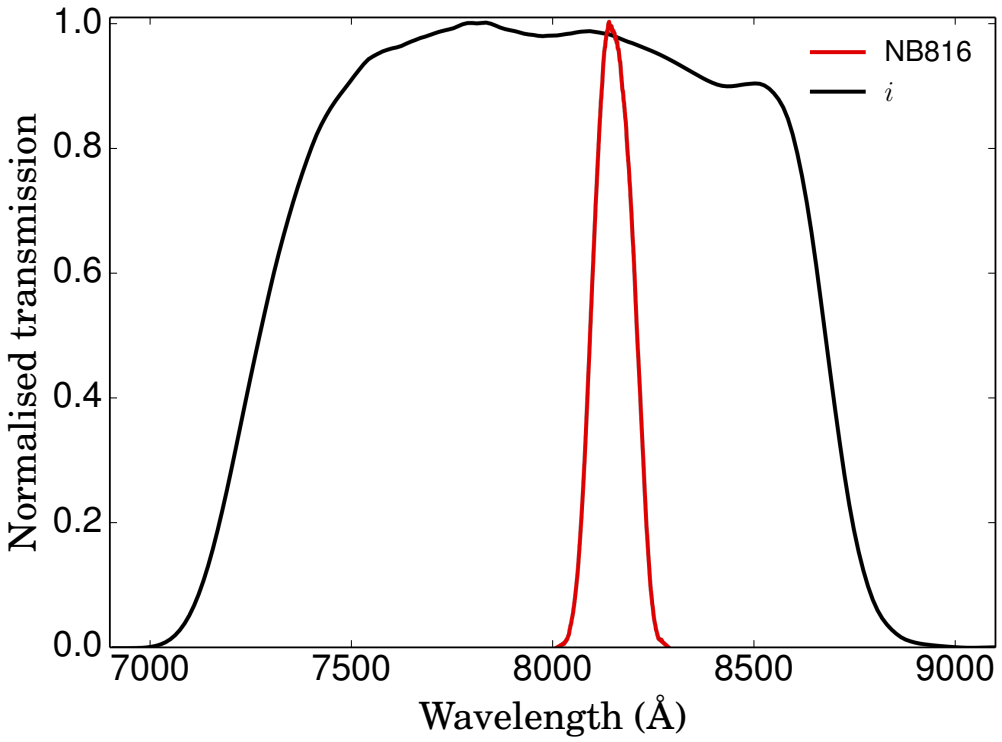

Figure 3.1: Normalised filter profiles of the NB816 and the i band filters used in this study. We note that the shown i band is for Subaru's Suprime-Cam after the upgrade to red sensitive CCDs, such that its peak is slightly shifted towards the red compared to the CFHT MegaCam i band used for SA22. Our NB correction in Section 3.4.1 takes this into account. NB816 is contained slightly red from the center of i. The NB816 filter is located in a wavelength region free of strong atmospheric OH lines.

Table 3.2: Multi-wavelength depths (2σ; measured in $2''$ empty apertures) for the available broad-band filters across all three fields.

Field	**Broad band filters**	**Broad band depth (2σ, $2''$)**
COSMOS	$BVgrizYJHK$	27.6, 27.0, 27.1, 27.0, 26.6, 25.7, 25.3, 24.6, 25.0, 24.7
UDS	$BVrizJK$	27.5, 27.2, 27.0, 26.8, 27.0, 25.3, 24.8
SA22	$ugrizJK$	26.2, 26.5, 25.9, 25.6, 24.5, 24.3, 23.8

any distortions along the CCD.

We calibrated the photometry in our data by matching relatively bright, un-saturated stars and galaxies to public catalogues for COSMOS (Laigle et al., 2016), UDS (Cirasuolo et al., 2007) and SA22 (Sobral et al., 2013, 2015; Matthee et al., 2014) using STILTS (Taylor, 2006). NB816 images were calibrated using i band photometry, but a further correction to this calibration was applied in Section 3.4.1. Co-added stacks of NB816 exposures were obtained using the SWARP software (Bertin et al., 2002).

We masked low quality regions, bright haloes around bright stars, diffraction patterns and low S/N regions due to dithering strategy (particularly important in SA22-wide). We also removed regions with low quality or absent i band coverage, regardless of the quality of the narrow band.

We note that our masking is very conservative and, consequently, a relatively large area is removed from our study (hundreds of arcmin^2), but that is still only a small fraction of our total area. After masking low quality regions, our NB816 coverage contains a total area of $7\,\mathrm{deg}^2$ (Figure 3.2), corresponding to a comoving volume of $6.3 \times 10^6\,\mathrm{Mpc}^3$ at $z = 5.7$. All areas and volumes used and mentioned in this dissertation take into account these masks, unless stated otherwise.

Finally, we measure the depth of our images using randomly placed $2''$ apertures. In each image, we place 200,000 empty apertures in random positions. The average results per field are given in Table 3.1.

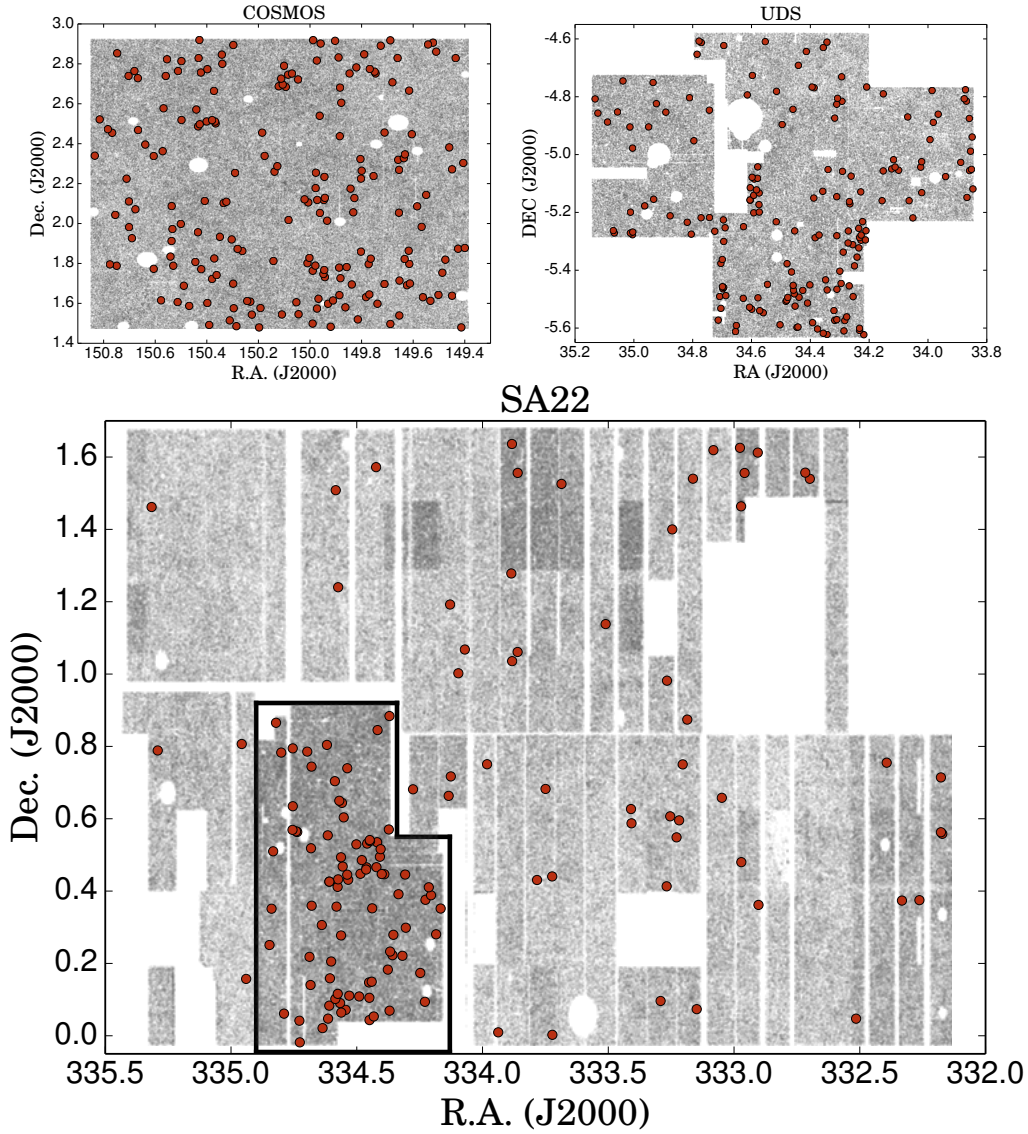

Figure 3.2: The spatial distribution of sources in the COSMOS, UDS and SA22 fields. Grey dots indicate all detections and red circles identify our $z = 5.7$ Lyα emitter candidates. A black line contour identifies SA22-deep, the deepest region in the SA22 field. The figure also highlights the regions masked due to bright stars, bad regions and/or low S/N due to dither strategy. It can be seen that UDS, COSMOS and SA22-deep are the deepest regions with a high concentration of sources and candidate LAEs.

3.3 Multi-wavelength imaging

A large collection of multi-wavelength data are publicly available for our entire coverage. For the COSMOS field, we use optical *BVgriz* data taken with the Subaru/SuprimeCam (Taniguchi et al., 2007; Capak et al., 2007), retrieved from the COSMOS Archive and NIR *YHJK* data from UltraVISTA DR2 (McCracken et al., 2012), taken with VISTA/VIRCAM. For the UDS field, we use optical *BVriz* data from SXDF (Furusawa et al., 2008) and NIR *JHK* data from UKIDSS (Lawrence et al., 2007). For the SA22 field we use optical *ugriz* data from CFHTLS[3], taken with the MegaCam (Boulade et al., 2003) and NIR *JK* data from UKIDSS DXS (Warren et al., 2007), taken with UKIRT/WFCAM (Casali et al., 2007). All data which were not taken with the Subaru/SuprimeCam were degraded to a pixel scale of $0.20''\,\mathrm{pix}^{-1}$ using SWARP. A summary of the available filters for each field and their photometric depth is shown in Table 3.2.

3.4 NB816 catalogue

The extraction of sources was conducted using SExtractor (Bertin and Arnouts, 1996) in dual extraction mode, using NB816 as the detection image. We used a detection threshold of 1.5 (scaling factor to the background RMS), an analysis threshold of 1.5 (in surface brightness, relative to the background rms), a minimum of four pixels above threshold triggering detection, subtraction of the internal, automatically interpolated background-map, a magnitude zeropoint of 30 (set by calibration), gaussian filter (5×5 convolution mask of a gaussian PSF with FWHM = 2.0 pixels) and a pixel scale of $0.20''\,\mathrm{pix}^{-1}$.

3.4.1 Narrow band magnitude correction

The NB816 filter is located slightly to the red of the Subaru Suprime-cam i filter (with red sensitive CCDs) with a separation of $\approx 180\,\text{Å}$ between the center of the two filters. Calibrating the narrow band magnitude directly to the i band may result in an offset in the magnitudes, particularly for sources

[3] http://www.cfht.hawaii.edu/Science/CFHTLS/

with strong colours. We correct the narrow band magnitudes by summing a small correction factor which is estimated from the color of the two adjacent broad bands, i and z. To compute this correction, we use sources with i, z and NB816 magnitudes between 19 and 24 (not saturated and with high enough S/N). The correction has the following expression:

$$NB_{corrected} = NB + 0.4 \times (i - z), \tag{3.1}$$

where NB, i and z are the $2''$ magnitudes in the respective bands and $NB_{corrected}$ is the corrected NB816 magnitude. We apply this correction to sources with i and z detections. For the remaining sources, we apply a median correction of +0.20. As a result of this correction, there is less scatter in the excess diagram (Figure 4.1). The correction also corrects for the fact that the CFHT MegaCam i band is slightly bluer than Suprime-cam's i band, because this slightly different i band will result in slightly different $i - z$ colours.

Our narrow band correction is an alternative to the correction applied in Murayama et al. (2007) who used a corrected broad band obtained from an iz interpolation. Our narrow band correction corresponds to a $BB_{corrected} = 0.6i + 0.4z$ which is fully consistent with their interpolation.

3.4.2 Removal of sources with non-physical narrow band detection

The wavelengths covered by NB816 are contained inside the i band coverage. This means that sources with NB816 detection should be detected in i as long as the i image is deep enough. For each source we compute the expected i magnitude if it only had emission inside NB816. If the measured i magnitude of a source is fainter than this value and the depth of the i image is sufficient to detect it, we remove it from our sample. This step mainly removes variable sources (such as supernovae and moving sources) and spurious sources that are detected only in the narrow band images and sources with boosted narrow band emission from e.g. diffraction patterns.

3.4.3 Cosmic ray removal

Cosmic rays may become artefacts in images. This problem can be avoided through stacking of several frames. However, in our shallower SA22-wide data, the small number of frames causes a less efficient removal of such artefacts during stacking. We created an automated procedure to identify and remove cosmic rays from our sample.

For each source detected in the NB816 imaging we measure the standard deviation in boxes of 5×5 pixels around each source. Cosmic rays can be easily identified by their high standard deviation, several times higher than any real source. We apply a cautious cut to make sure we do not lose any real sources. Since we were cautious with this step, we also visually inspect all the final LAE candidates to identify any cosmic ray that was not excluded.

Chapter 4

Selection of sources

4.1 Selecting NB816 line-emitters

For the selection of line-emitters, we apply similar criteria to e.g. Sobral et al. (2013) and Matthee et al. (2015), relying on two parameters: equivalent width (EW) and Sigma (Σ). These parameters are explained in detail in section 2.1.

To select our sample of line-emitters, we apply the following selection criteria:

- $i - NB816 > 0.8$
- $\Sigma > 3$

The narrow band excess criteria $i - NB816 > 0.8$ corresponds to a rest-frame EW of 25 Å for a $z = 5.7$ LAE. This cut is similar to the one used by Hu et al. (2010) and Matthee et al. (2015) for $z = 6.6$ but slightly lower than e.g. Ouchi et al. (2008) ($i - NB816 > 1.2$) and Taniguchi et al. (2005) ($i - NB816 > 1$).

We present the narrow band excess diagram in Figure 4.1, highlighting our sample of line-emitters. With our selection criteria we identify over 11,000 candidate line-emitters.

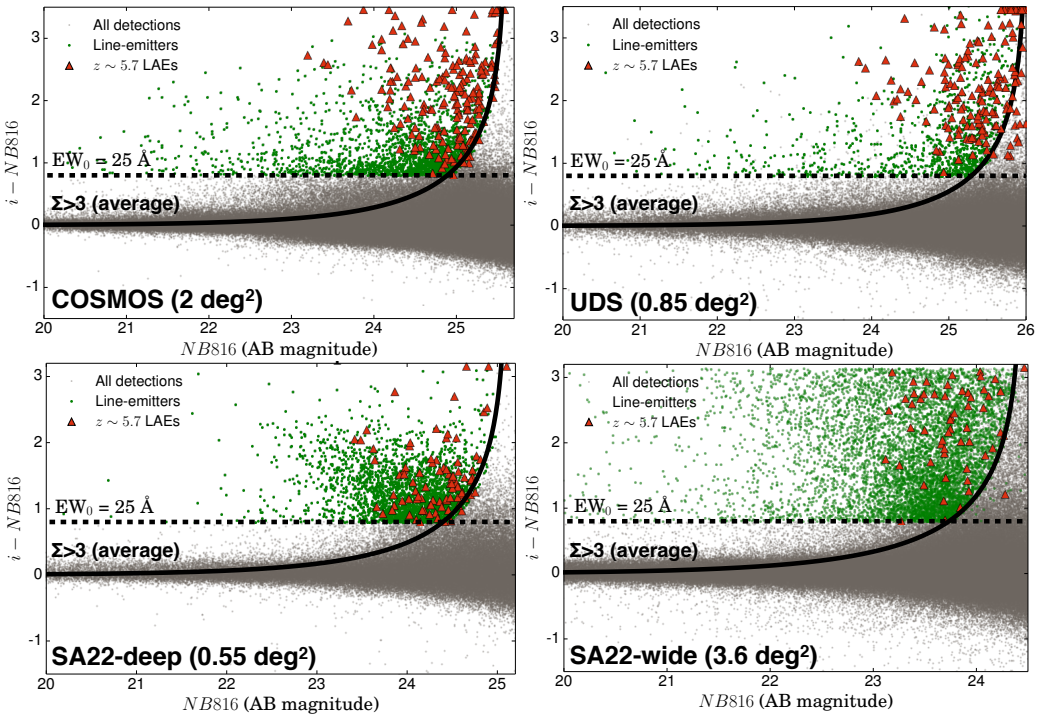

Figure 4.1: Narrow band excess diagram for COSMOS, UDS and SA22. We plot narrow band excess (i broad band magnitude minus NB816 magnitude) versus narrow band NB816 magnitude. Grey points represent all detections after masking, removal of sources with non-physical narrow band and cosmic rays. Green points represent line-emitters, obtained by applying the EW and Σ cuts described in Section 4.1. For visual reference, we collapsed the points with no i detection in the top region of the plots. The Σ line shown in this figure is the median value from small sub-fields which we created inside each field.

4.2 Photometric and spectroscopic redshifts

In order to explore the nature of the line-emitters, we have used accurate photometric redshifts and a large compilation of spectroscopic redshifts: Laigle et al. (2016) for COSMOS, Cirasuolo et al. (2007) for UDS and a combination of Kim et al. (2015), Matthee et al. (2014) and Sobral et al. (2015) for SA22. We retrieve ~ 5000 emitters with either available photometric or spectroscopic redshift. Figure 4.2 presents the distribution of photometric redshifts of our sample of line-emitters. Even though our high EW cut is tuned to select Lyα emitters at $z = 5.7$, our initial sample of line-emitters reveals a range of strong line-emitters. The peaks in the photometric redshifts are consistent with Hα at $z \sim 0.2$, [OIII] at ~ 0.6, [OII] at $z \sim 1.2$ and Lyα at $z = 5.7$. From our spectroscopic redshift, we find a total of 46 Lyα emitters at $z = 5.7$.

As expected, our sample is dominated by lower redshift line-emitters, mostly composed by sources up to $z \sim 1.2$. In order to isolate LAEs at z= 5.7 from our sample we require additional selection criteria, which we will explore in Section 4.3.

4.3 Selection of LAEs at z = 5.7

In order to select Lyα emitters and remove low redshift interlopers, we use the Lyman break technique (detailed in section 2.2) and identify the break at rest frame 912 Å, blue-ward of the Lyman limit (although, in practice, at $z = 5.7$, radiation blue-ward of Lyα is almost fully absorbed by the Lyα forest; e.g. Madau 1995). LAEs at $z = 5.7$ should have no strong detection in optical wavelengths below the i band. A weak r band detection is possible if the IGM is relatively transparent (and there are few Lyα forest lines). To summarise, we apply the following criteria, similar to Ouchi et al. (2008):

$$B > B_{2\sigma} \wedge V > V_{2\sigma} \wedge [r > r_{2\sigma} \vee (r < r_{2\sigma} \wedge r - i > 1.0)] \qquad (4.1)$$

Where B, V, r and i are the $2''$ magnitudes in the respective bands and the $_{2\sigma}$ subscript indicates the 2σ depth for the images of the respective bands (see Table 3.2). As there are no available BV data over the full SA22, we

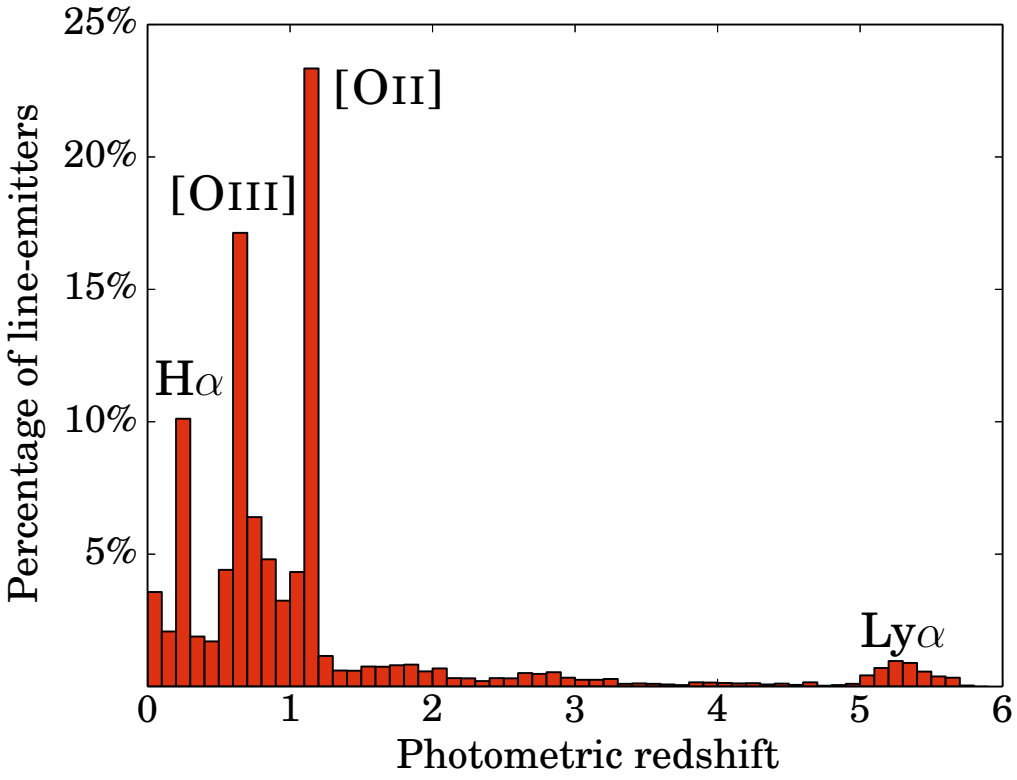

Figure 4.2: Distribution of photometric redshifts of line-emitters selected in COSMOS, UDS and SA22 by using a simple selection criteria of $i - NB186 > 0.25$ and $\Sigma > 3$. The peaks are consistent with line-emission at specific wavelengths. Annotations indicate the redshifts where we expect major emission lines (Hα at $z \sim 0.2$, [OIII] at ~ 0.6, [OII] at $z \sim 1.2$ and Lyα at $z = 5.7$).

apply a small variation of Equation 4.1 where we use ug instead:

$$u > u_{2\sigma} \wedge g > g_{2\sigma} \wedge [r > r_{2\sigma} \vee (r < r_{2\sigma} \wedge r - i > 1.0)] \tag{4.2}$$

Where u, g are the $2''$ magnitudes in the respective bands. This criteria ensures we select sources with no detection in the $BVug$ bands but can have some detection in r as long as there is a strong $i - r$ color break.

In extreme cases, $z \sim 1$ line-emitters with a strong Balmer-break could mimic the Lyman-break that we detect. Fortunately, those sources can be identified by their red colors. Similar to Matthee et al. (2015) we reject sources which have significant red colors in the observed NIR bands. Thus, we consider sources with $J - K > 0.5$ to be interlopers. This additional NIR criterion is most important in SA22, where the optical data are relatively shallow.

In order to ensure that our candidates are real detections and not spurious sources, we visually inspect each one of the remaining candidates. We first inspect sources in the narrow band images and reject any fake detections (usually originated by e.g. diffraction patterns from bright sources which were not completely masked). We also visually check that each source does not have an optical detection blue-ward of the Lyman-break. To do so, we create an optical stack using the available optical bands for each field (BVg for COSMOS, BV for UDS and ug for SA22), which significantly increases the depth of our images.

To summarise, we select line-emitters as Lyα at $z = 5.7$ if:

- They have no optical detection blue-ward of the Lyman-break (Equation 4.1 or 4.2).
- They satisfy $J - K < 0.5$, if detected in the NIR.
- They pass visual inspection, which includes both reality of NB excess (and checking for variability and/or moving sources) and no detection in optical bands.

4.4 Comparison with other samples of Lyα emitters at z = 5.7

We compare our sample of LAEs with the spectroscopically confirmed sources at $z = 5.7$ provided by Ouchi et al. (2008) (UDS), Hu et al. (2010) (SA22-deep) and Mallery et al. (2012) (COSMOS). We find that we recover 46 spectroscopically confirmed sources from previous studies which are above our conservative Σ detection threshold (other studies typically only apply an EW cut) and that are not in our conservative masked regions.

4.5 Final sample of Lyα emitters at z = 5.7

Across the COSMOS, UDS and SA22 fields we identify a total of 514 $z = 5.7$ LAE candidates (currently 46 are spectroscopically confirmed), spanning a range of Lyα luminosities of $10^{42.5} - 10^{44}\,\mathrm{erg\,s^{-1}}$. We will explore the properties of these sources in the following sections. Table 4.1 shows a summary of the number of sources after each selection criterion. The spatial distribution of the LAEs in all fields can be seen in Figure 3.2.

Table 4.1: Number of candidates after each selection step. The visual inspections step includes individually checking each source first in both the narrow band NB816 and the broad band i images and then for no detection in the deep optical stacks (BV for UDS, BVg for COSMOS and ug for SA22). Note that due to the shallower broad band data in SA22, a large amount of sources passed the initial filtering, but are rejected with the much deeper ug stacks and our visual checks.

COSMOS	**# sources**
$\Sigma > 3$, $\mathrm{EW}_0 > 25\,\mathrm{\AA}$	2576
No optical detection	396
After visual inspections	192
UDS	
$\Sigma > 3$, $\mathrm{EW}_0 > 25$	981
No optical detection	239
After visual inspections	178
SA22-wide	
$\Sigma > 3$, $\mathrm{EW}_0 > 25$	4692
No optical detection	1264
After visual inspections	56
SA22-deep	
$\Sigma > 3$, $\mathrm{EW}_0 > 25$	2803
No optical detection	541
After visual inspections	88
Total Lyα z = 5.7 ($\mathbf{z_{spec}}$ confirmed)	514 (46)

Chapter 5

Computing the Lyα Luminosity Function

In this chapter we compute the Lyα LF, i.e., the distribution of the number density of sources as a function of their Lyα luminosity. We apply corrections to the LF which we explore in the following sections.

We determine Lyα luminosities by converting line-fluxes using:

$$L_{\mathrm{Ly}\alpha} = 4\pi D_L^2 f_{\mathrm{Ly}\alpha} \tag{5.1}$$

Where $D_L = 54363$ Mpc is the luminosity distance at $z = 5.7$, $f_{\mathrm{Ly}\alpha}$ is the Lyα line-flux obtained with 2" apertures and $L_{\mathrm{Ly}\alpha}$ is the Lyα luminosity.

The line-flux of a source (f_{line}) can be expressed as:

$$f_{line} = \Delta\lambda_{NB} \frac{f_{NB} - f_{BB}}{1 - \frac{\Delta\lambda_{NB}}{\Delta\lambda_{BB}}} \tag{5.2}$$

Where $\Delta\lambda_{NB}$ and $\Delta\lambda_{BB}$ are the FWHM of the narrow band and broad band filters ($\Delta\lambda_{NB816}$ =120 Å; $\Delta\lambda_i$ =1349 Å) and f_{NB} and f_{BB} are the flux densities measured in the two filters.

5.1 Completeness correction

Faint sources and sources with weak emission lines may be missed by our selection criteria, causing the measured number density of sources to be underestimated. To estimate the line-flux completeness we follow Sobral et al.

(2013), adapted for Lyα studies by Matthee et al. (2015): we construct a sample of high-redshift non line-emitters selected through a simple color break selection ($r-i > 1.5$) and add non-emitters with photometric or spectroscopic redshift higher than 4. Using these sources, in steps of increasing line-flux, we artificially increase their NB816 and i band fluxes and then apply our selection criteria on these simulated sources. By determining the fraction that we retrieve as a function of added line-flux, we obtain a completeness estimation for each luminosity bin, which we apply to each bin in our LF. A higher completeness correction is measured for the fainter sources as they are much easier to be missed. The completeness corrected number counts in the different observed fields as a function of their Lyα luminosity are shown in Figure 6.1 and in Table 6.2.

5.2 Filter profile correction

The narrow band filter transmission NB816 has a gaussian distribution with a lower transmission in the wings (Figure 3.1). Sources which have a redshift in the borders of the filter will only be observed at a fraction of their Lyα luminosity (see e.g. Hu et al., 2010). It is necessary to apply a correction factor that compensates the fact that the filter is not top-hat, otherwise, the number densities of bright LAEs will be systematically underestimated. We apply a correction similar to Matthee et al. (2015). We use the Schechter fit from our data to generate the Lyα luminosity of 1 million sources at a random redshift between $z = 5.65$ and $z = 5.75$ (corresponding to the edges of NB816). For each luminosity bin, the correction factor is determined from the detection ratio of these fake sources retrieved with the two different filter profiles. The effect of the filter profile correction of our LF is shown in Figure 6.2. The correction is higher for the brightest bins as these LAEs will likely be observed at a fraction of their luminosity due to the filter not being top-hat.

5.3 Aperture corrections

Due to instrumental/observational effects (e.g. seeing/PSF) and mostly due to Lyα photons easily scattering within haloes, Lyα flux can be significantly extended (e.g. Momose et al., 2014; Wisotzki et al., 2016; Matthee et al.,

2016b; Borisova et al., 2016). The 2″ apertures we use are $3-4\times$ the PSF, and thus for point-like sources we do not expect aperture corrections to be important, but if sources are physically extended, 2″ apertures may lead to missing flux. We investigate this by comparing the NB816 fluxes measured in 2″ with those measured with MAG-AUTO and study any necessary correction as a function of observed 2″ flux. We find little to no dependence up to at least the highest fluxes, and derive a median correction of +0.02 in Lyα luminosity, which we apply (see further discussion in Section 6.3).

5.4 Interloper correction

While in COSMOS and UDS the available broad-band data allows to clearly identify and remove interlopers/lower redshift line-emitters, in SA22 this is not necessarily the case, particularly for the sources with the faintest continuum. In order to mitigate this, we use our combined COSMOS and UDS with full information, but study the dataset assuming the depths of broad-band imaging were the same as SA22-deep and SA22-wide. We find that, as expected, the contamination is higher (10% higher) for SA22-like data-sets. We therefore correct all our luminosity bins in SA22 for this expected extra contamination.

5.5 Obtaining a comparison LF at z = 6.6

In order to compare our results at $z = 5.7$, we explore the results and sample presented by Matthee et al. (2015) and apply any necessary corrections/modifications to derive a new, updated $z = 6.6$ LF. We use the same methods for completeness and filter profile corrections. We compute the errors per bin by not only taking into account the Poissonian errors, but also by considering systematic errors due to the completeness and filter profile corrections. Furthermore, following our selection criteria, we also carefully check for any variable sources and/or moving sources which can contaminate the bright end. Matthee et al. (2015) applied a statistical correction for these potential contaminants, but we chose to investigate sources one by one, following what we do at $z = 5.7$. We note that such statistical correction works very well for COSMOS and UDS, but is a slight underestimation for SA22,

as the number of moving sources in SA22 is significantly higher. Nonetheless, we find that none of the results of Matthee et al. (2015), which are based spectroscopic follow-up (Sobral et al., 2015) are significantly changed. We note that we also apply an aperture correction to the $z = 6.6$ LF of $+0.11$, unchanged from Matthee et al. (2015).

5.6 Filter profile corrections and LFs

Figure 6.2 shows the effect of our filter profile corrections. We show the completeness corrected number densities of LAEs in bins of Lyα luminosity for individual fields at $z = 5.7$ (Table 6.1) and for the combined coverage at $z = 5.7$ and $z = 6.6$ (Table 6.2).

5.7 Schechter Function

The Schechter function (Schechter, 1976) is a common parametrization of the LF which consists of a power-law at faint luminosities and an exponential drop at bright luminosities. It is defined by three parameters: the power-law slope α, the characteristic number density $\phi^\star$ and the characteristic luminosity $L^\star$. It has the expression:

$$\phi(L)dL = \phi^\star(L/L^\star)^\alpha \exp(-L/L^\star)d(L/L^\star) \tag{5.3}$$

Chapter 6

Results

6.1 The z = 5.7 Lyα luminosity function

6.1.1 Field to field variations

We group our LAEs in luminosity bins according to their Lyα luminosity. The observed number density in each bin is corrected for its corresponding line-flux completeness correction. We only include sources from sub-fields with a completeness higher than 25%. The number density for each luminosity bin is calculated by multiplying the number of counts by the completeness factor, divided by the probed volume and bin width. The errors are Poissonian, but we add 30% of the completeness correction in quadrature to obtain the final error per bin.

In Figure 6.1 we show the $z = 5.7$ Lyα luminosity computed per field. We find that there is significant scatter, of the order of ± 0.4 dex in the number densities, at least for the range of luminosities where we can compare results from all our fields. It may well be that such scatter is reduced for fainter sources, but our sample does not allow us to constrain that as we can only investigate that with a single field (UDS) – see Ouchi et al. (2008). Our results per field are also presented in Table 6.1. Our results highlight the importance of probing multiple fields and caution the over-interpretation of single field "over" or "under" densities, either in the context of reionization or of structure formation.

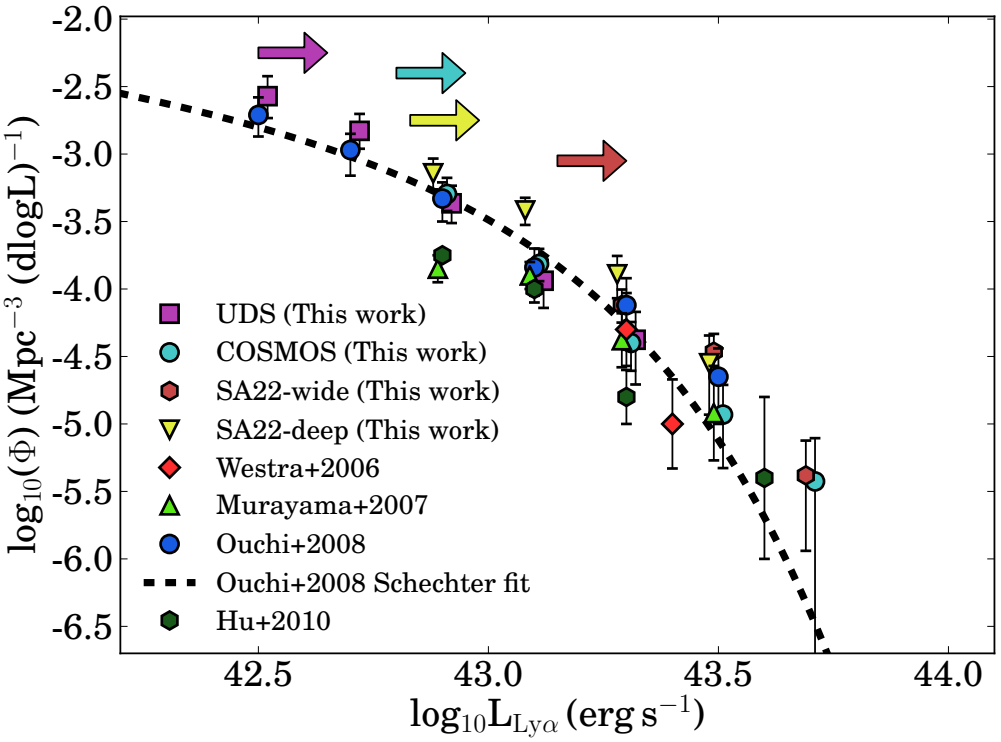

Figure 6.1: The Lyα luminosity function at $z = 5.7$ based on different fields. For visual reference, a small offset in the luminosities (± 0.02 dex) was used to minimize overlapping of points in the figure. The arrows indicate the luminosity bins for which each field has an average completeness higher than 25%. We find significant field to field variations of ± 0.4 dex in number densities, consistent with results from e.g. Ouchi et al. (2008). We also compare our results per field with previous studies, finding them to be consistent with Murayama et al. (2007) and Ouchi et al. (2008). However, by probing larger, multiple volumes we overcome cosmic variance.

Table 6.1: The completeness corrected number density of LAEs in the different surveyed fields at $z = 5.7$.

Field	**Luminosity bin** $\log_{10}$L [erg s^{-1}]	**Number density** $\log_{10}\Phi$/dlogL [Mpc^{-3}]
UDS	42.5 ± 0.1	$-2.57^{+0.15}_{-0.16}$
	42.7 ± 0.1	$-2.82^{+0.13}_{-0.13}$
	42.9 ± 0.1	$-3.37^{+0.13}_{-0.15}$
	43.1 ± 0.1	$-3.94^{+0.16}_{-0.20}$
	43.3 ± 0.1	$-4.37^{+0.21}_{-0.33}$
COSMOS	42.9 ± 0.1	$-3.30^{+0.12}_{-0.13}$
	43.1 ± 0.1	$-3.81^{+0.11}_{-0.13}$
	43.3 ± 0.1	$-4.40^{+0.16}_{-0.21}$
	43.5 ± 0.1	$-4.93^{+0.22}_{-0.39}$
	43.7 ± 0.1	$-5.42^{+0.32}_{-\infty}$
SA22-deep	42.9 ± 0.1	$-3.09^{+0.11}_{-0.12}$
	43.1 ± 0.1	$-3.37^{+0.09}_{-0.11}$
	43.3 ± 0.1	$-3.84^{+0.14}_{-0.18}$
	43.5 ± 0.1	$-4.50^{+0.21}_{-0.38}$
SA22-wide	43.3 ± 0.1	$-4.07^{+0.11}_{-0.13}$
	43.5 ± 0.1	$-4.41^{+0.13}_{-0.16}$
	43.7 ± 0.1	$-5.33^{+0.26}_{-0.56}$

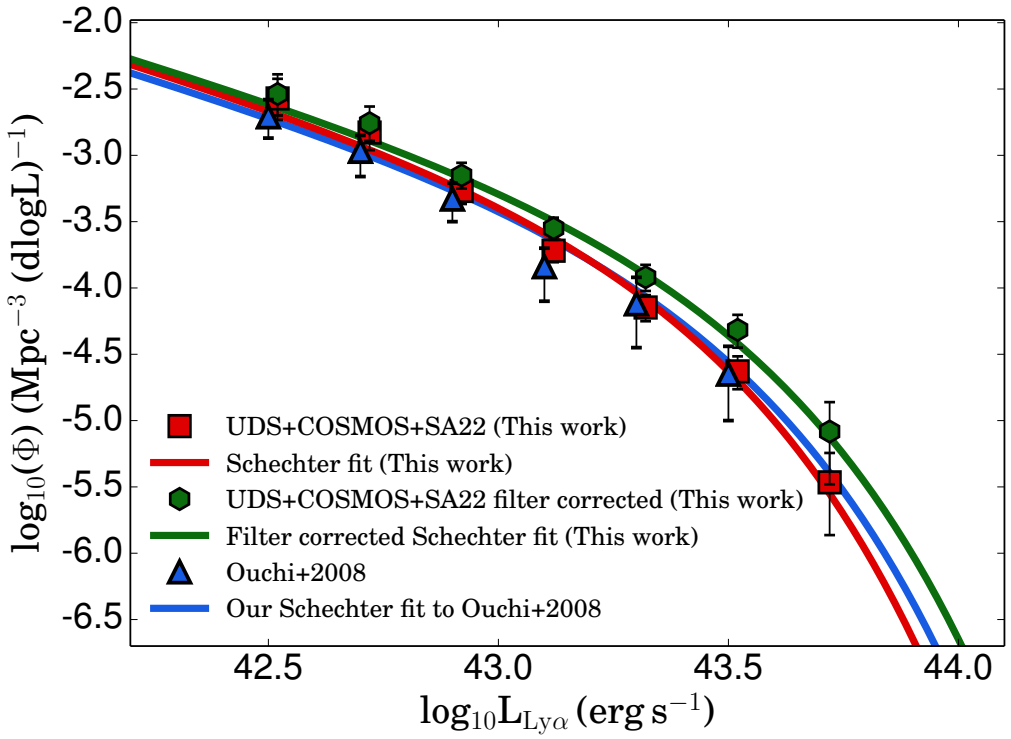

Figure 6.2: The number densities in luminosity bins from our survey in the UDS, COSMOS and SA22 fields (red squares) and the bins from Ouchi et al. (2008) in blue triangles. A small luminosity correction of +0.02 was applied to our luminosity bins to correct for extended emission (this correction is discussed in §6.3). The Schechter fits to the luminosity bins from our study agrees very well with Ouchi et al. (2008). In green we also show the luminosity bins from this work after we apply a filter profile bias correction (we estimate this correction in §5.2) and the corrected LF Schechter fit. The effect of this correction is strongest at the brightest bins.

6.1.2 Comparison with other $z = 5.7$ surveys

Several surveys have published LFs of $z = 5.7$ LAEs, which we compare with our results (see Figure 6.1). We compare our results with Westra et al. (2006), Murayama et al. (2007) (COSMOS), Ouchi et al. (2008) (UDS) and Hu et al. (2010) (SA22-deep, SSA17, A370 and GOODS-N) in Figure 6.1. While there are some differences between our selection criteria and the ones applied in these studies, overall we find very good agreement. Moreover, the variance that we see from field to field (see Figure 6.1) is sufficient to explain any subtle differences between our results per field and those in the literature.

For the COSMOS field, Murayama et al. (2007) applies a much more conservative Σ cut (corresponding to roughly $\Sigma > 5$) which leads to missing fainter LAEs. The different Σ cut, together with a different completeness correction (ours is based on line-flux or luminosity, while Murayama et al. 2007 does a correction based on detection completeness) easily explains why our fainter luminosity bin ($\log_{10}\mathrm{L}_{\mathrm{Ly}\alpha} = 42.9\,\mathrm{erg\,s^{-1}}$) has a higher number density, which fully agrees with our UDS and SA22 estimates, along with those presented in Ouchi et al. (2008).

Within the errors, our results are also fully consistent with those by Ouchi et al. (2008), at all luminosities. Our brightest bin ($\log_{10}\mathrm{L}_{\mathrm{Ly}\alpha} = 43.7\,\mathrm{erg\,s^{-1}}$) is populated only by our COSMOS and SA22-wide fields, as those have the largest areas (sufficiently large to probe the bright end), but we note that the estimates from COSMOS and SA22-wide fully agree, while we are also in very good agreement with the results from Hu et al. (2010). SA22-deep is both our smallest contiguous field and also the one with the highest number densities (although generally agreeing within the errors with the other fields, particularly given the variance seen). In the SA22-wide field we find number densities consistent with Ouchi et al. (2008) up to $\log_{10}\mathrm{L}_{\mathrm{Ly}\alpha} = 43.5$ erg s^{-1} and a brighter bin consistent with our COSMOS number density. The bright end of the Lyα LF seems to point towards a deviation from the Schechter fit presented in Ouchi et al. (2008), better explained by a less accentuated exponential drop, or by a single power-law.

6.1.3 The combined $z = 5.7$ Lyα luminosity function

We combine our data from the different fields to obtain a combined Lyα luminosity function at $z = 5.7$. We show the results in Figure 6.3 and Table 6.2.

We fit a Schechter function (Schechter, 1976), defined by three parameters: the power-law slope α, the characteristic number density $\phi^\star$ and the characteristic luminosity $L^\star$.

In Table 6.3, we present best-fit parameters of the Schechter function at $z = 5.7$. We find the faint end slope α to be particularly steep: $\alpha = -2.3^{+0.4}_{-0.3}$. This is in very good agreement with recent results from Dressler et al. (2015) at the same redshift who found α to be $-2.35 < \alpha < -1.95$ (while we find $-2.6 < \alpha < -1.9$, $1\,\sigma$). It is therefore clear that the Lyα luminosity function is very steep just after re-ionisation and may be steeper than the UV luminosity function at the same redshift ($\alpha \approx -1.9$; e.g. Bouwens et al., 2015). Note that such a steep faint-end slope at $z = 5.7$ is already preferred by the fit in Ouchi et al. (2008) and is consistent with theoretical expectations (Gronke et al., 2015).

We also fit our LF by fixing the faint-end slope to $\alpha = -2.0$ and $\alpha = -1.5$ and allow $\Phi^\star$ and $L^\star$ to vary. This allow our results to be directly compared with other studies which fixed α to the same values. The results are presented in Table 6.3.

6.2 Evolution from z = 5.7 to z ∼ 7 and beyond

In Section 5.5 we discuss the steps we took to obtain a comparable and updated $z = 6.6$ Lyα luminosity function, based on Matthee et al. (2015). We show the recomputed $z = 6.6$ Lyα LF, and a comparison with our $z = 5.7$ measurement in Figure 6.3. The recomputed $z = 6.6$ LF is fully presented in Table 6.2.

We find that both $z = 6.6$ and $z = 5.7$ are best fit with a very steep α of ~ -2.3. At a fixed α, our results show a significant decline in the number density of the more "typical"/faint Lyα emitters from $z = 5.7$ to $z = 6.6$, with ϕ^* declining by 0.5 dex. However, and in very good agreement with Matthee

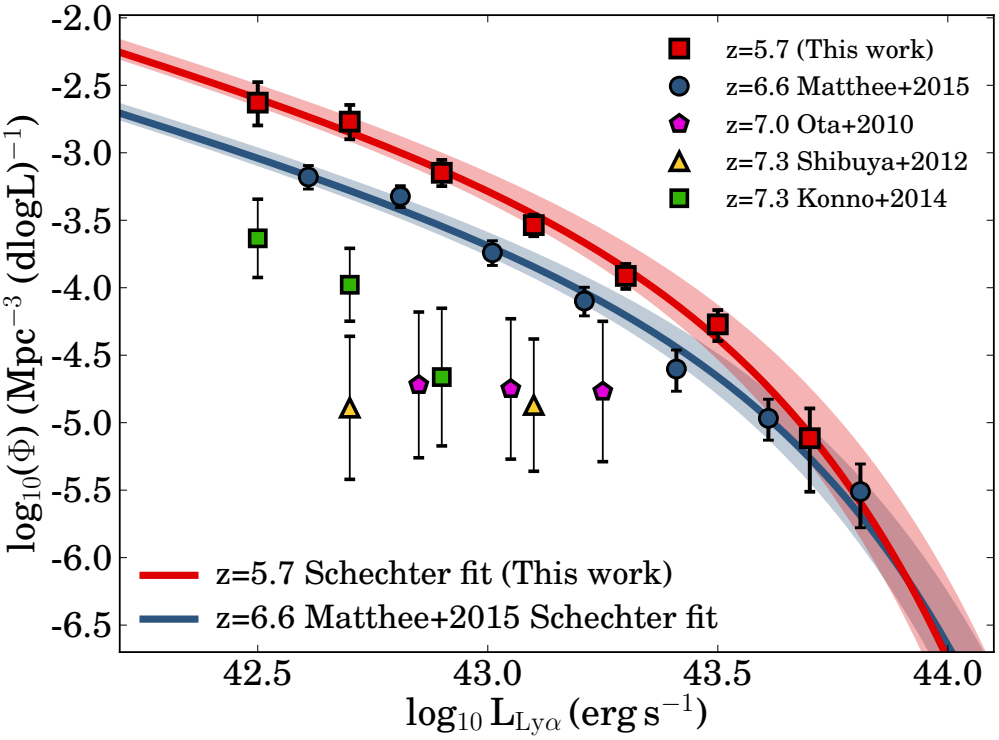

Figure 6.3: Evolution of the Lyα LF from $z = 5.7$ to $z = 6.6$. The $z = 6.6$ LF is our updated version from Matthee et al. (2015), see Section 5.5. The colored regions around the best Schechter fit show the 1σ error in L^*. We observe a strong decrease in the number density of the fainter LAEs as we increase with redshift up to $z = 6.6$ and also $z > 7$ (Ota et al., 2010; Shibuya et al., 2012; Konno et al., 2014). This decrease can likely be explained by a more neutral IGM as we go deeper into the reionization epoch. However, there seems to be no evolution for the brighter sources, which can likely be explained by a preferential reionization around the brightest sources. There is currently a lack of comparable surveys at $z > 7$ at the brightest luminosities.

Table 6.2: The completeness and filter profile bias corrected luminosity functions at $z = 5.7$ and $z = 6.6$ from this study. Note that we corrected the bins for extended emission (see Section 6.3).

Redshift	**Luminosity bin** $\log_{10}$L [erg s^{-1}]	**Volume** [10^6 Mpc^3]	**Observed number density** $\log_{10}\Phi$/dlogL [Mpc^{-3}]	**Corrected number density** $\log_{10}\Phi$/dlogL [Mpc^{-3}]
$\boldsymbol{z = 5.7}$	42.52 ± 0.1	0.19	$-3.16^{+0.08}_{-0.09}$	$-2.63^{+0.16}_{-0.17}$
	42.72 ± 0.1	0.65	$-3.32^{+0.05}_{-0.06}$	$-2.77^{+0.12}_{-0.13}$
	42.92 ± 0.1	3.09	$-3.65^{+0.04}_{-0.04}$	$-3.15^{+0.10}_{-0.10}$
	43.12 ± 0.1	3.09	$-3.89^{+0.05}_{-0.05}$	$-3.54^{+0.08}_{-0.08}$
	43.32 ± 0.1	6.30	$-4.34^{+0.05}_{-0.06}$	$-3.91^{+0.09}_{-0.10}$
	43.52 ± 0.1	6.30	$-4.70^{+0.08}_{-0.10}$	$-4.27^{+0.11}_{-0.12}$
	43.72 ± 0.1	6.30	$-5.62^{+0.20}_{-0.37}$	$-5.12^{+0.22}_{-0.40}$
$\boldsymbol{z = 6.6}$	42.61 ± 0.1	0.38	$-3.46^{+0.09}_{-0.08}$	$-3.18^{+0.08}_{-0.09}$
	42.81 ± 0.1	0.64	$-3.59^{+0.08}_{-0.07}$	$-3.32^{+0.08}_{-0.08}$
	43.01 ± 0.1	1.07	$-4.01^{+0.11}_{-0.09}$	$-3.74^{+0.09}_{-0.10}$
	43.21 ± 0.1	1.73	$-4.42^{+0.14}_{-0.11}$	$-4.10^{+0.10}_{-0.11}$
	43.41 ± 0.1	1.73	$-4.94^{+0.30}_{-0.18}$	$-4.60^{+0.14}_{-0.16}$
	43.61 ± 0.1	4.18	$-5.34^{+0.31}_{-0.18}$	$-4.97^{+0.14}_{-0.16}$
	43.81 ± 0.1	4.18	$-5.97^{+0.31}_{-0.26}$	$-5.51^{+0.20}_{-0.26}$

Table 6.3: Parameters for the best Schechter function fits for the Lyα LFs at $z = 5.7$ and $z = 6.6$ (recomputed Matthee et al., 2015). We allow α to vary, but we also fix α to -2.0 and -1.5.

Redshift	α	$\mathbf{\log_{10}L^\star_{Ly\alpha}}$ (erg s^{-1})	$\mathbf{\log_{10}\Phi^\star}$ (Mpc^{-3})
$\boldsymbol{z = 5.7}$	$-2.3^{+0.4}_{-0.3}$	$43.42^{+0.50}_{-0.22}$	$-4.02^{+0.48}_{-0.93}$
	-1.5 (fix)	$43.06^{+0.05}_{-0.04}$	$-3.25^{+0.09}_{-0.10}$
	-2.0 (fix)	$43.25^{+0.09}_{-0.06}$	$-3.63^{+0.12}_{-0.16}$
$\boldsymbol{z = 6.6}$	$-2.3^{+0.4}_{-0.3}$	$43.45^{+0.35}_{-0.18}$	$-4.48^{+0.43}_{-0.68}$
	-1.5 (fix)	$43.12^{+0.04}_{-0.03}$	$-3.73^{+0.07}_{-0.06}$
	-2.0 (fix)	$43.30^{+0.07}_{-0.05}$	$-4.13^{+0.10}_{-0.10}$

et al. (2015), we find little to no evolution at the bright end, with L^* showing no significant evolution, or only a very weak increase of $\sim 0.05-0.1$ dex from $z = 5.7-6.6$ (depending on α). In practice, our results show that the number density of bright Lyα emitters ($L_{Ly\alpha} > 10^{43.5}\,erg\,s^{-1}$) shows no significant evolution from $z = 5.7$ to $z = 6.6$, confirming the results suggested in Matthee et al. (2015). We note that while we discuss the luminosity functions in the context of their Schechter fits, the results presented hold if we fit them with e.g. single or double power-laws. At $z = 6.6$, the spectroscopic confirmation of the sources responsible for these high Lyα luminosities is starting to reveal their uniqueness (e.g. multi-component, very low metallicities, blue Lyα wings, range of sizes, see e.g. Himiko, MASOSA, CR7, COLA1; Ouchi et al., 2013; Sobral et al., 2015; Hu et al., 2016), providing important hints that may explain how these sources have been able to likely reionize their surroundings already at $z \sim 7$. Further observations will be able to confirme a larger, statistical sample at $z \sim 7$, but our new sample at $z = 5.7$ is uniquely suited to be directly compared.

Figure 6.3 also presents results from several $z > 7$ narrow band surveys from the literature, which we compare with $z = 6.6$ and $z = 5.7$. The trend that we see from $z = 5.7$ to $z = 6.6$ of significant decrease in the number density of faint Lyα emitters seems to continue at a fast pace to $z \sim 7$ and beyond (Ota et al., 2010; Shibuya et al., 2012; Konno et al., 2014). We provide a more detailed discussion about the differential evolution of the Lyα as an imprint of reionization in Section 7. There is currently a lack of comparable surveys at $z > 7$ at the brightest luminosities, so it is not yet possible to test whether the lack of evolution at the bright end still holds at $z > 7$.

6.3 The Lyα sizes and evolution at z = 5.7 − 6.6

Since the Lyα transition is resonant, Lyα photons scatter in a medium with neutral hydrogen. Because of this, Lyα photons tend to escape over much large radii than their UV and Hα counterparts, making them observable as Lyα haloes (e.g. Rauch et al., 2008; Steidel et al., 2011; Momose et al., 2014;

Matthee et al., 2016b). Therefore, the aperture that is used to measure Lyα is critical (e.g. Wisotzki et al., 2016). Typically, LAE surveys have attempted to take extended Lyα emission into account by using MAG-AUTO measurements (e.g. Ouchi et al., 2010; Konno et al., 2016) or relatively large apertures (e.g. Murayama et al., 2007; Hu et al., 2010, who use $3''$ apertures at $z = 5.7$). However, the total measured magnitude with MAG-AUTO depends on the depth of the narrow-band imaging, such that a comparison between surveys and redshifts is challenging, particularly as Wisotzki et al. (2016) show that Lyα extends well beyond the typical limiting surface brightness of narrow-band surveys.

While we use fixed $2''$ apertures in similar excellent seeing conditions at both $z = 5.7$ and $z = 6.6$ (as this allows to understand the completeness and selection function in an optimal way; c.f. Matthee et al. 2015), we correct for any flux missed as described in Section 5.3.

Matthee et al. (2015) found that $2''$ apertures systematically underestimate Lyα luminosities at $z = 6.6$ (compared to the MAG-AUTO) with a median offset of 0.11 dex over the spectroscopically confirmed sample of LAEs (confirmed in Ouchi et al. 2010). Here we extend this analysis to the full sample of sources at both $z = 5.7$ and $z = 6.6$. We find that the median offset between the MAG-AUTO luminosity and the $2''$ aperture offset at $z = 6.6$ is 0.11 dex, while it is only 0.02 dex at $z = 5.7$; see Figure 6.4. The latter explains why our $2''$ measurements result in very similar number densities as literature studies with larger apertures at $z = 5.7$, see Fig. 6.1.

By splitting the sample of LAEs in bins of Lyα luminosity (in $2''$ apertures), we find that at $z = 5.7$ the offset increases slightly with increasing Lyα luminosity (see Fig. 6.4). Specifically, the most luminous LAEs have larger Lyα haloes (and more flux at larger radii) than the typical fainter ones. Interestingly, we find a different behaviour at $z = 6.6$. While the brightest $z = 6.6$ Lyα seem to be as extended as those at $z = 5.7$ (these are the ones that may have already been able to fully ionise the surrounding environment), fainter Lyα emitters at $z = 6.6$ are all more extended than comparable sources at $z = 5.7$. Together with the differential evolution of the Lyα LF, our results provide strong evidence for reionization effects being much stronger for the faint sources than for the bright ones. We discuss this

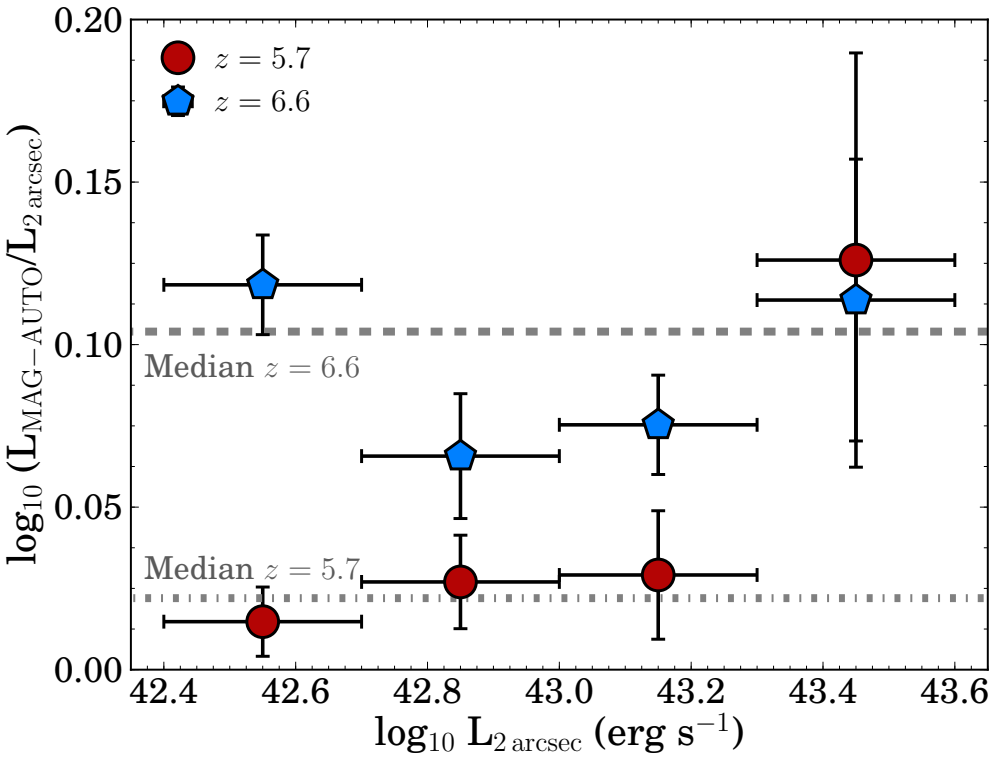

Figure 6.4: The median difference in MAG-AUTO luminosity and luminosity within 2″ apertures in bins of the 2″ aperture Lyα luminosity for LAE samples at $z = 5.7$ and $z = 6.6$. The dashed and dashed-dotted grey lines indicate the median of all LAEs in the sample, which is obviously dominated by low luminosity sources. At both redshifts, more centrally luminous LAEs also have relatively more flux at larger radii (which is captured by MAG-AUTO). At faint central luminosities LAEs at $z = 6.6$ appear more extended, which could be due to increased scattering in HI around galaxies. We note that this may be one of the causes for the apparent evolution in the Lyα LF, and may also be important to consider when interpreting the spectroscopic follow-up of UV-selected galaxies with low Lyα luminosities, as slits will recover even less of the total flux.

trend further in Section 7.

A similar but more careful analysis of the extent of Lyα emission at $z = 5.7 - 6.6$ than our own has been done by Momose et al. (2014), who created stacked narrow band and broad band images of the LAEs in UDS from Ouchi et al. (2008, 2010). They observed that Lyα is extended, being more extended than their UV counterpart (while also being more extended than the PSF of their images). They find evidence for an increase in the scale length of Lyα from $z = 5.7$ to $z = 6.6$. However, they did not separate their sample in bins of luminosity and their results are obtained with median stacking. This means that the faintest sources dominate (as there are more faint sources than luminous ones) and that these results are more representative of a "typical" LAE, with $L_{Ly\alpha} \sim 10^{42.6}\,\mathrm{erg\,s^{-1}}$. The median evolution in the scale length of Lyα haloes from LAEs estimated in Momose et al. (2014) is thus consistent with the difference between MAG-AUTO and $2''$ measurements that we find for relatively faint LAEs between $z = 5.7$ and $z = 6.6$.

Chapter 7

Discussion: Imprints from reionization?

As noted before, the observed Lyα luminosity at a fixed spatial scale is expected to decrease in the reionization era, as an increasingly neutral IGM scatters Lyα photons into larger, extended haloes (e.g. Dijkstra, 2014). Our results are consistent with witnessing such predictions directly. Here we discuss the differences we observe in the Lyα luminosity function between $z = 5.7$ and $z = 6.6$, and also our results on the extent of Lyα emitters at $z = 5.7$ and $z = 6.6$. For earlier work, see e.g. Dijkstra et al. (2007), Ouchi et al. (2010) and Hu et al. (2010).

We observe strong differential evolution of the Lyα LF from $z \sim 6$ to $z \sim 7$, with a significant decrease (-0.5 dex) in the number density for Lyα luminosities below L^*. The drop in the observability of faint LAEs may well be explained by a larger fraction of neutral IGM at $z > 6$ caused by reionization not being completed. The brightest emitters would not suffer from such a decline because their strong Lyα emission is easier to be observed, as previously illustrated by the simple toy model in Matthee et al. (2015). This model assumes that the Lyα luminosity scales with the ionising output and LAEs are only observed if they are either capable of ionising the IGM around them, or are strongly clustered. To first order, a stronger ionising output for brighter LAEs is expected because Lyα is a recombination line (such that at fixed escape fraction, a higher Lyα luminosity scales with the number of ionising photons). Also, as shown in Matthee et al. (2016a), LAEs at $z = 2.2$ typically produce more ionising photons per unit UV luminosity

than more typical galaxies such as Hα emitters (HAEs). Furthermore, as hypothesised by Dijkstra and Gronke (2016), ISM conditions which favor the escape of Lyα photons also likely favor the escape of Lyman continuum (LyC) photons (for example due to a porous ISM), such that in addition to producing more ionising photons, LAEs could also leak more ionising photons into the IGM.

Recent evidence from Stark et al. (2016) shows that the fraction of bright UV selected galaxies (LBGs) with strong Lyα emission is much higher than was previously found (e.g. Schenker et al., 2014; Pentericci et al., 2014; Schmidt et al., 2016) when they are selected on strong nebular lines (e.g. Hβ/[OIII]). This is likely because UV-bright galaxies are in over-dense regions and emit copious amount of ionising radiation (inferred from observed high ionization UV lines as CIII] and their high EW optical nebular lines). Such conditions may also favor the production of Lyα photons and lead to larger ionised bubbles. Therefore, these observations are in principle consistent with the observed evolution of the Lyα LF, where we observe reionization completing first around luminous LAEs.

A unique benefit of narrow-band Lyα observations over (slit) spectroscopy is that narrow-band imaging gives information on the spatial extent of Lyα emission, which could be connected to the neutral fraction of the IGM (e.g. Dijkstra and Loeb, 2008). As we show in Figure 6.4, we find that the median difference between $2''$ apertures and the total magnitude (as observed with MAG-AUTO) is much smaller at $z = 5.7$ than at $z = 6.6$. Most interestingly, the major difference is found at the faintest luminosities. At $z = 6.6$, LAEs which have a low central luminosity have a relatively much larger total luminosity than at $z = 5.7$. This means that at a fixed surface brightness limit (note that the limiting surface brightness at $z = 6.6$ is actually even slightly higher), faint LAEs are more extended at $z = 6.6$ than at $z = 5.7$. For more luminous LAEs the difference is much smaller. This effect can easily be explained in the framework of the Matthee et al. (2015) toy-model: faint LAEs are surrounded by a relatively more neutral IGM, such that there is more resonant scattering leading to more extended emission.

The evolution of the Lyα LF and the extent of Lyα for different luminosities may very well be explained by a patchy reionization scenario where

the IGM is ionised first around luminous LAEs. However, internal effects from galaxies may also be important. Furthermore, studying the clustering of both bright and faint LAEs and how it evolves from e.g. $z = 5.7$ to $z = 6.6$ and beyond (e.g. Mesinger, 2010; Ouchi et al., 2010) will provide the extra, necessary constraints. A similar analysis with future larger samples of LAEs (for example from the Hyper Suprime Cam survey) will be very useful to confirm the observed trends.

Our results also mean that a careful approach is required in order to interpret the observed Lyα fraction for samples of LBGs at different redshifts in terms of a varying neutral fraction due to reionization, because different subsets of LBGs show very different Lyα fractions. Moreover, our results show that typical, faint Lyα emitters become more extended as we go into the reionization epoch, with the same (or even less) flux being spread over larger areas. This is an additional challenge for the traditional slit spectroscopy follow-up, which will struggle to detect any Lyα if the flux is significantly extended.

Chapter 8

Conclusions

We have constructed the largest Lyα narrow band survey at $z = 5.7$, when re-ionization is close to complete. We have surveyed a total area of $7\,\mathrm{deg}^2$ and a volume of $6.3 \times 10^6 \mathrm{Mpc}^3$ at $z = 5.7$, covering the COSMOS, UDS and SA22 fields. Here we summarize the main conclusions:

- By identifying strong line-emitters with a Lyman break, we find 514 LAE candidates at $z = 5.7$ with $\mathrm{EW}_0 > 25$ Å ($\mathrm{EW}_0 \sim 25 - 1000$ Å) and luminosities ranging from $10^{42.5} - 10^{44}$ erg s^{-1}, in a single, homogeneous data-set.

- We find that cosmic variance plays a major role, with variations of ± 0.4 dex in number densities of Lyα emitters from field to field.

- By combining all our fields and overcoming cosmic variance, we find that the faint end slope of the $z = 5.7$ Lyα luminosity function is very steep, with $\alpha = -2.3^{+0.4}_{-0.3}$. If we fix $\alpha = -2.0$, we find $L^\star = 10^{43.22^{+0.08}_{-0.05}}\,\mathrm{erg\,s^{-1}}$ and $\Phi^\star = -3.60^{+0.12}_{-0.16}\,\mathrm{Mpc^{-3}}$.

- We also present an updated $z = 6.6$ Lyα luminosity function, based on comparable volumes, and obtained with the same methods, which we directly compare with that at $z = 5.7$.

- We find significant evolution from $z = 5.7$ (after re-ionization) to $z = 6.6$ (within the epoch of re-ionization) at the faint end. We find that the fainter the luminosity, the stronger the drop in the number density

of Lyα emitters. The strong decrease of the number density of faint Lyα emitters continues to $z \sim 7$.

- At bright Lyα luminosities ($L_{Ly\alpha} > 10^{43.5}\,erg\,s^{-1}$) we find no evolution in the number density of Lyα emitters when we enter the re-ionization era. This is consistent with bright Lyα emitters being preferentially observable because they already are in ionized bubbles even at $z \sim 7$.

- Faint Lyα emitters at $z = 6.6$ show more extended haloes than those at $z = 5.7$, suggesting that neutral Hydrogen plays a more important role of scattering Lyα photons at $z = 6.6$.

All together, our results indicate that we are observing patchy reionization happening first around the brightest Lyα emitters, allowing the number densities of those sources to remain unaffected by the increase of neutral Hydrogen from $z \sim 5$ to $z \sim 7$. We observe a preferential evolution of the faint end of the Lyα LF from $z = 5.7$ to $z = 6.6$. There is a decrease in the faint end while the bright end shows little to no evolution. We also observe no evolution in the sizes of the brighter emitters, which could be interpreted as showing no evidence of extra scattering around them from $z = 5.7$ to $z = 6.6$, while faint sources show a significant difference, presenting much more flux at larger radii. The spectroscopic confirmation of relatively bright Lyα emitters beyond $z \sim 7$ and approaching $z \sim 9$ (Oesch et al., 2015; Zitrin et al., 2015) may already be hinting that our results may hold to even higher redshifts.

The nature and diversity of bright Lyα sources at $z = 6.6$, which we find to have essentially the same number density as those at $z = 5.7$, are starting to be unveiled. Spectroscopic follow up (e.g. Ouchi et al., 2013; Sobral et al., 2015; Zabl et al., 2015; Hu et al., 2016), detailed modelling (e.g. Hartwig et al., 2015; Dijkstra et al., 2016; Agarwal et al., 2016; Visbal et al., 2016; Smidt et al., 2016; Smith et al., 2016) and other observations with HST and ALMA (Ouchi et al., 2013; Sobral et al., 2015; Schaerer et al., 2015; Bowler et al., 2016) are revealing a surprising diversity. Current results indicate that these sources may have a range of powering sources (from metal poor populations to multiple stellar populations and also AGN, including potentially direct collapse black holes). Regardless of their nature, their observability requires the production and emission of the necessary amount of ionising LyC photons

capable of ionising a large enough local bubble to make them observable as bright Lyα sources already at $z = 6.6$. Thus, even though these sources are not as abundant as the more typical, faint sources, they may well play an important role in cosmic reionization, at least at very early stages, a scenario which would be in agreement with what is seen by Matthee et al. (2016a). Further observations of our sample of bright $z = 5.7$ sources and of much larger, statistical samples at $z \sim 5 - 7$ will certainly shed light over many of the current open questions, while the availability of JWST will provide a revolutionary window into the physical conditions within these sources.

8.1 Future work

Extensive follow-up work can be carried out from the study in this dissertation.

The obvious first step is to study in detail the large sample of LAEs that we have selected at $z = 5.7$ and $z = 6.6$. We are currently conducting spectroscopic follow-up observations of our sources and we have already confirmed two new extremely luminous sources, one at each redshift. Moreover, HST time has already been granted to follow up our brightest targets, with observations being taken early next year. This will give extremely valuable insight in the properties of this sources, such as equivalent width and extended emission.

The next step is to expand our searches, both in area (with e.g. the new Hyper Suprime-Cam instrument from the Subaru Telescope) and more redshift slices (wide narrow band surveys have not been conducted with all the narrow band filters shown in 2.1). Wide areas reduce cosmic variance and allow us to find the brightest (also rarer) sources. Additional redshift slices allow us to more efficiently probe the evolution of LAEs across cosmic time. We have already been granted 44 hours to conduct a wide $z = 7.7$ Lyα pilot study (over COSMOS) with the HAWK-I instrument from the VLT.

With our collection of extremely bright sources, we can effectively constrain how deep surveys need to be in order to detect such sources. This results in efficient survey planning which can optimize our searches.

References

J. J. Adams et al. The HETDEX Pilot Survey. I. Survey Design, Performance, and Catalog of Emission-line Galaxies. *ApJS*, 192:5, January 2011. doi: 10.1088/0067-0049/192/1/5.

B. Agarwal, J. L. Johnson, E. Zackrisson, I. Labbe, F. C. van den Bosch, P. Natarajan, and S. Khochfar. Detecting Direct Collapse Black Holes: making the case for CR7. *MNRAS*, May 2016. doi: 10.1093/mnras/stw1173.

R. Amanullah, C. Lidman, D. Rubin, G. Aldering, P. Astier, K. Barbary, M. S. Burns, A. Conley, K. S. Dawson, S. E. Deustua, M. Doi, S. Fabbro, L. Faccioli, H. K. Fakhouri, G. Folatelli, A. S. Fruchter, H. Furusawa, G. Garavini, G. Goldhaber, A. Goobar, D. E. Groom, I. Hook, D. A. Howell, N. Kashikawa, A. G. Kim, R. A. Knop, M. Kowalski, E. Linder, J. Meyers, T. Morokuma, S. Nobili, J. Nordin, P. E. Nugent, L. Östman, R. Pain, N. Panagia, S. Perlmutter, J. Raux, P. Ruiz-Lapuente, A. L. Spadafora, M. Strovink, N. Suzuki, L. Wang, W. M. Wood-Vasey, N. Yasuda, and T. Supernova Cosmology Project. Spectra and Hubble Space Telescope Light Curves of Six Type Ia Supernovae at 0.511 $<$ z $<$ 1.12 and the Union2 Compilation. *ApJ*, 716:712–738, June 2010. doi: 10.1088/0004-637X/716/1/712.

Astropy Collaboration, T. P. Robitaille, E. J. Tollerud, P. Greenfield, M. Droettboom, E. Bray, T. Aldcroft, M. Davis, A. Ginsburg, A. M. Price-Whelan, W. E. Kerzendorf, A. Conley, N. Crighton, K. Barbary, D. Muna, H. Ferguson, F. Grollier, M. M. Parikh, P. H. Nair, H. M. Unther, C. Deil, J. Woillez, S. Conseil, R. Kramer, J. E. H. Turner, L. Singer, R. Fox, B. A. Weaver, V. Zabalza, Z. I. Edwards, K. Azalee Bostroem, D. J. Burke, A. R.

Casey, S. M. Crawford, N. Dencheva, J. Ely, T. Jenness, K. Labrie, P. L. Lim, F. Pierfederici, A. Pontzen, A. Ptak, B. Refsdal, M. Servillat, and O. Streicher. Astropy: A community Python package for astronomy. *A&P*, 558:A33, October 2013. doi: 10.1051/0004-6361/201322068.

R. Bacon, J. Brinchmann, J. Richard, T. Contini, A. Drake, M. Franx, S. Tacchella, J. Vernet, L. Wisotzki, J. Blaizot, N. Bouché, R. Bouwens, S. Cantalupo, C. M. Carollo, D. Carton, J. Caruana, B. Clément, S. Dreizler, B. Epinat, B. Guiderdoni, C. Herenz, T.-O. Husser, S. Kamann, J. Kerutt, W. Kollatschny, D. Krajnovic, S. Lilly, T. Martinsson, L. Michel-Dansac, V. Patricio, J. Schaye, M. Shirazi, K. Soto, G. Soucail, M. Steinmetz, T. Urrutia, P. Weilbacher, and T. de Zeeuw. The MUSE 3D view of the Hubble Deep Field South. *A&P*, 575:A75, March 2015. doi: 10.1051/0004-6361/201425419.

M. B. Bayliss, E. Wuyts, K. Sharon, M. D. Gladders, J. F. Hennawi, B. P. Koester, and H. Dahle. Two Lensed Lyman-α Emitting Galaxies at z˜ 5. *ApJ*, 720:1559–1568, September 2010. doi: 10.1088/0004-637X/720/2/1559.

G. D. Becker, J. S. Bolton, P. Madau, M. Pettini, E. V. Ryan-Weber, and B. P. Venemans. Evidence of patchy hydrogen reionization from an extreme Lyα trough below redshift six. *MNRAS*, 447:3402–3419, March 2015. doi: 10.1093/mnras/stu2646.

R. H. Becker, X. Fan, R. L. White, M. A. Strauss, V. K. Narayanan, R. H. Lupton, J. E. Gunn, J. Annis, N. A. Bahcall, J. Brinkmann, A. J. Connolly, I. Csabai, P. C. Czarapata, M. Doi, T. M. Heckman, G. S. Hennessy, Ž. Ivezić, G. R. Knapp, D. Q. Lamb, T. A. McKay, J. A. Munn, T. Nash, R. Nichol, J. R. Pier, G. T. Richards, D. P. Schneider, C. Stoughton, A. S. Szalay, A. R. Thakar, and D. G. York. Evidence for Reionization at z˜6: Detection of a Gunn-Peterson Trough in a z=6.28 Quasar. *AJ*, 122:2850–2857, December 2001. doi: 10.1086/324231.

C. L. Bennett, A. J. Banday, K. M. Gorski, G. Hinshaw, P. Jackson, P. Keegstra, A. Kogut, G. F. Smoot, D. T. Wilkinson, and E. L. Wright.

Four-Year COBE DMR Cosmic Microwave Background Observations: Maps and Basic Results. *ApJL*, 464:L1, June 1996. doi: 10.1086/310075.

E. Bertin. Automatic Astrometric and Photometric Calibration with SCAMP. In C. Gabriel, C. Arviset, D. Ponz, and S. Enrique, editors, *Astronomical Data Analysis Software and Systems XV*, volume 351 of *Astronomical Society of the Pacific Conference Series*, page 112, July 2006.

E. Bertin and S. Arnouts. SExtractor: Software for source extraction. *A&PS*, 117:393–404, June 1996. doi: 10.1051/aas:1996164.

E. Bertin, Y. Mellier, M. Radovich, G. Missonnier, P. Didelon, and B. Morin. The TERAPIX Pipeline. In D. A. Bohlender, D. Durand, and T. H. Handley, editors, *Astronomical Data Analysis Software and Systems XI*, volume 281 of *Astronomical Society of the Pacific Conference Series*, page 228, 2002.

G. A. Blanc et al. The HETDEX Pilot Survey. II. The Evolution of the Lyα Escape Fraction from the Ultraviolet Slope and Luminosity Function of 1.9 $<$ z $<$ 3.8 LAEs. *ApJ*, 736:31, July 2011. doi: 10.1088/0004-637X/736/1/31.

E. Borisova et al. Ubiquitous giant Lyman α nebulae around the brightest quasars at $z \sim 3.5$ revealed with MUSE. *ArXiv e-prints*, May 2016.

O. Boulade, X. Charlot, P. Abbon, S. Aune, P. Borgeaud, P.-H. Carton, M. Carty, J. Da Costa, H. Deschamps, D. Desforge, D. Eppellé, P. Gallais, L. Gosset, R. Granelli, M. Gros, J. de Kat, D. Loiseau, J.-. Ritou, J. Y. Roussé, P. Starzynski, N. Vignal, and L. G. Vigroux. MegaCam: the new Canada-France-Hawaii Telescope wide-field imaging camera. In M. Iye and A. F. M. Moorwood, editors, *Instrument Design and Performance for Optical/Infrared Ground-based Telescopes*, volume 4841 of *Proc. SPIE*, pages 72–81, March 2003. doi: 10.1117/12.459890.

R. J. Bouwens, G. D. Illingworth, P. A. Oesch, M. Trenti, I. Labbé, L. Bradley, M. Carollo, P. G. van Dokkum, V. Gonzalez, B. Holwerda, M. Franx, L. Spitler, R. Smit, and D. Magee. UV Luminosity Functions

at Redshifts z $\sim$ 4 to z $\sim$ 10: 10,000 Galaxies from HST Legacy Fields. *ApJ*, 803:34, April 2015. doi: 10.1088/0004-637X/803/1/34.

R. A. A. Bowler, J. S. Dunlop, R. J. McLure, and D. J. McLeod. Unveiling the nature of bright z ˜ 7 galaxies with the Hubble Space Telescope. *ArXiv e-prints*, May 2016.

G. B. Brammer, P. G. van Dokkum, and P. Coppi. EAZY: A Fast, Public Photometric Redshift Code. *ApJ*, 686:1503-1513, October 2008. doi: 10.1086/591786.

A. J. Bunker, S. J. Warren, P. C. Hewett, and D. L. Clements. On near-infrared Hα searches for high-redshift galaxies. *MNRAS*, 273:513–516, March 1995. doi: 10.1093/mnras/273.2.513.

P. Capak, H. Aussel, M. Ajiki, H. J. McCracken, B. Mobasher, N. Scoville, P. Shopbell, Y. Taniguchi, D. Thompson, S. Tribiano, S. Sasaki, A. W. Blain, M. Brusa, C. Carilli, A. Comastri, C. M. Carollo, P. Cassata, J. Colbert, R. S. Ellis, M. Elvis, M. Giavalisco, W. Green, L. Guzzo, G. Hasinger, O. Ilbert, C. Impey, K. Jahnke, J. Kartaltepe, J.-P. Kneib, J. Koda, A. Koekemoer, Y. Komiyama, A. Leauthaud, O. Le Fevre, S. Lilly, C. Liu, R. Massey, S. Miyazaki, T. Murayama, T. Nagao, J. A. Peacock, A. Pickles, C. Porciani, A. Renzini, J. Rhodes, M. Rich, M. Salvato, D. B. Sanders, C. Scarlata, D. Schiminovich, E. Schinnerer, M. Scodeggio, K. Sheth, Y. Shioya, L. A. M. Tasca, J. E. Taylor, L. Yan, and G. Zamorani. The First Release COSMOS Optical and Near-IR Data and Catalog. *ApJS*, 172:99–116, September 2007. doi: 10.1086/519081.

P. L. Capak et al. Galaxies at redshifts 5 to 6 with systematically low dust content and high [C II] emission. *Nature*, 522:455–458, June 2015. doi: 10.1038/nature14500.

M. Casali, A. Adamson, C. Alves de Oliveira, O. Almaini, K. Burch, T. Chuter, J. Elliot, M. Folger, S. Foucaud, N. Hambly, M. Hastie, D. Henry, P. Hirst, M. Irwin, D. Ives, A. Lawrence, K. Laidlaw, D. Lee, J. Lewis, D. Lunney, S. McLay, D. Montgomery, A. Pickup, M. Read,

N. Rees, I. Robson, K. Sekiguchi, A. Vick, S. Warren, and B. Woodward. The UKIRT wide-field camera. *A&P*, 467:777–784, May 2007. doi: 10.1051/0004-6361:20066514.

P. Cassata et al. The VIMOS VLT Deep Survey: star formation rate density of Lyα emitters from a sample of 217 galaxies with spectroscopic redshifts 2 < z z 6.6. *A&A*, 525:A143, January 2011. doi: 10.1051/0004-6361/201014410.

P. Cassata et al. The VIMOS Ultra-Deep Survey (VUDS): fast increase in the fraction of strong Lyman-α emitters from z = 2 to z = 6. *A&A*, 573: A24, January 2015. doi: 10.1051/0004-6361/201423824.

R. Cen and Z. Haiman. Quasar Strömgren Spheres Before Cosmological Reionization. *ApJL*, 542:L75–L78, October 2000. doi: 10.1086/312937.

S. Charlot and S. M. Fall. Lyman-Alpha Emission from Galaxies. *ApJ*, 415: 580, October 1993. doi: 10.1086/173187.

M. Cirasuolo, R. J. McLure, J. S. Dunlop, O. Almaini, S. Foucaud, I. Smail, K. Sekiguchi, C. Simpson, S. Eales, S. Dye, M. G. Watson, M. J. Page, and P. Hirst. The evolution of the near-infrared galaxy luminosity function and colour bimodality up to z ˜= 2 from the UKIDSS Ultra Deep Survey Early Data Release. *MNRAS*, 380:585–595, September 2007. doi: 10.1111/j.1365-2966.2007.12038.x.

L. L. Cowie and E. M. Hu. High-z Lyalpha Emitters. I. A Blank-Field Search for Objects near Redshift Z = 3.4 in and around the Hubble Deep Field and the Hawaii Deep Field SSA 22. *AJ*, 115:1319–1328, April 1998. doi: 10.1086/300309.

M. Dijkstra. Lyα Emitting Galaxies as a Probe of Reionisation. *PASA*, 31: e040, October 2014. doi: 10.1017/pasa.2014.33.

M. Dijkstra and M. Gronke. The LyA-LyC Connection: Evidence for an Enhanced Contribution of UV-faint Galaxies to Cosmic Reionization. *ArXiv e-prints*, April 2016.

M. Dijkstra and A. Loeb. The polarization of scattered Lyα radiation around high-redshift galaxies. *MNRAS*, 386:492–504, May 2008. doi: 10.1111/j.1365-2966.2008.13066.x.

M. Dijkstra, A. Lidz, and J. S. B. Wyithe. The impact of The IGM on high-redshift Lyα emission lines. *MNRAS*, 377:1175–1186, May 2007. doi: 10.1111/j.1365-2966.2007.11666.x.

M. Dijkstra, M. Gronke, and D. Sobral. Lyα Signatures from Direct Collapse Black Holes. *ApJ*, 823:74, June 2016. doi: 10.3847/0004-637X/823/2/74.

A. Dressler, A. Henry, C. L. Martin, M. Sawicki, P. McCarthy, and E. Villaneuva. Confirmation of a Steep Luminosity Function for Lyα Emitters at z = 5.7: a Major Component of Reionization. *ApJ*, 806:19, June 2015. doi: 10.1088/0004-637X/806/1/19.

J. Dunkley, E. Komatsu, M. R. Nolta, D. N. Spergel, D. Larson, G. Hinshaw, L. Page, C. L. Bennett, B. Gold, N. Jarosik, J. L. Weiland, M. Halpern, R. S. Hill, A. Kogut, M. Limon, S. S. Meyer, G. S. Tucker, E. Wollack, and E. L. Wright. Five-Year Wilkinson Microwave Anisotropy Probe Observations: Likelihoods and Parameters from the WMAP Data. *ApJs*, 180:306–329, February 2009. doi: 10.1088/0067-0049/180/2/306.

J. S. Dunlop, R. J. McLure, B. E. Robertson, R. S. Ellis, D. P. Stark, M. Cirasuolo, and L. de Ravel. A critical analysis of the ultraviolet continuum slopes (β) of high-redshift galaxies: no evidence (yet) for extreme stellar populations at z $\gtrsim$ 6. *MNRAS*, 420:901–912, February 2012. doi: 10.1111/j.1365-2966.2011.20102.x.

J. S. Dunlop, R. J. McLure, A. D. Biggs, J. E. Geach, M. J. Michalowski, R. J. Ivison, W. Rujopakarn, E. van Kampen, A. Kirkpatrick, A. Pope, D. Scott, A. M. Swinbank, T. A. Targett, I. Aretxaga, J. E. Austermann, P. N. Best, V. A. Bruce, E. L. Chapin, S. Charlot, M. Cirasuolo, K. E. K. Coppin, R. S. Ellis, S. L. Finkelstein, C. C. Hayward, D. H. Hughes, E. Ibar, S. Khochfar, M. P. Koprowski, D. Narayanan, C. Papovich, J. A. Peacock, B. Robertson, T. Vernstrom, P. P. van der Werf, G. W. Wilson, and M. Yun. A deep ALMA image of the Hubble Ultra Deep Field. *ArXiv e-prints*, June 2016.

X. Fan, M. A. Strauss, R. H. Becker, R. L. White, J. E. Gunn, G. R. Knapp, G. T. Richards, D. P. Schneider, J. Brinkmann, and M. Fukugita. Constraining the Evolution of the Ionizing Background and the Epoch of Reionization with z˜6 Quasars. II. A Sample of 19 Quasars. *ApJ*, 132:117–136, July 2006. doi: 10.1086/504836.

S. L. Finkelstein, R. E. Ryan, Jr., C. Papovich, M. Dickinson, M. Song, R. S. Somerville, H. C. Ferguson, B. Salmon, M. Giavalisco, A. M. Koekemoer, M. L. N. Ashby, P. Behroozi, M. Castellano, J. S. Dunlop, S. M. Faber, G. G. Fazio, A. Fontana, N. A. Grogin, N. Hathi, J. Jaacks, D. D. Kocevski, R. Livermore, R. J. McLure, E. Merlin, B. Mobasher, J. A. Newman, M. Rafelski, V. Tilvi, and S. P. Willner. The Evolution of the Galaxy Rest-frame Ultraviolet Luminosity Function over the First Two Billion Years. *ApJ*, 810:71, September 2015. doi: 10.1088/0004-637X/810/1/71.

H. Furusawa, G. Kosugi, M. Akiyama, T. Takata, K. Sekiguchi, I. Tanaka, I. Iwata, M. Kajisawa, N. Yasuda, M. Doi, M. Ouchi, C. Simpson, K. Shimasaku, T. Yamada, J. Furusawa, T. Morokuma, C. M. Ishida, K. Aoki, T. Fuse, M. Imanishi, M. Iye, H. Karoji, N. Kobayashi, T. Kodama, Y. Komiyama, Y. Maeda, S. Miyazaki, Y. Mizumoto, F. Nakata, J. Noumaru, R. Ogasawara, S. Okamura, T. Saito, T. Sasaki, Y. Ueda, and M. Yoshida. The Subaru/XMM-Newton Deep Survey (SXDS). II. Optical Imaging and Photometric Catalogs. *ApJS*, 176:1-18, May 2008. doi: 10.1086/527321.

E. Glikman, S. G. Djorgovski, D. Stern, A. Dey, B. T. Jannuzi, and K.-S. Lee. The Faint End of the Quasar Luminosity Function at z ˜ 4: Implications for Ionization of the Intergalactic Medium and Cosmic Downsizing. *ApJL*, 728:L26, February 2011. doi: 10.1088/2041-8205/728/2/L26.

M. Gronke, M. Dijkstra, M. Trenti, and S. Wyithe. Connecting faint-end slopes of the Lyman α emitter and Lyman-break galaxy luminosity functions. *MNRAS*, 449:1284–1290, May 2015. doi: 10.1093/mnras/stv329.

J. E. Gunn and B. A. Peterson. On the Density of Neutral Hydrogen in Intergalactic Space. *ApJ*, 142:1633–1641, November 1965. doi: 10.1086/148444.

A. H. Guth. Inflationary universe: A possible solution to the horizon and flatness problems. *PRD*, 23:347–356, January 1981. doi: 10.1103/PhysRevD.23.347.

T. Hartwig, M. A. Latif, M. Magg, V. Bromm, R. S. Klessen, S. C. O. Glover, D. J. Whalen, E. W. Pellegrini, and M. Volonteri. Exploring the nature of the Lyman-α emitter CR7. *ArXiv e-prints*, December 2015.

M. Hayashi, D. Sobral, P. N. Best, I. Smail, and T. Kodama. Calibrating [O II] star formation rates at z $\sim$ 1 from dual Hα-[O II] imaging from HiZELS. *MNRAS*, 430:1042–1050, April 2013. doi: 10.1093/mnras/sts676.

M. Hayes, D. Schaerer, and G. Östlin. The H-alpha luminosity function at redshift 2.2 . A new determination using VLT/HAWK-I. *A&P*, 509:L5, January 2010. doi: 10.1051/0004-6361/200913217.

M. Hayes, D. Schaerer, G. Östlin, J. M. Mas-Hesse, H. Atek, and D. Kunth. On the Redshift Evolution of the Lyα Escape Fraction and the Dust Content of Galaxies. *ApJ*, 730:8, March 2011. doi: 10.1088/0004-637X/730/1/8.

K. Heitmann, M. White, C. Wagner, S. Habib, and D. Higdon. The Coyote Universe. I. Precision Determination of the Nonlinear Matter Power Spectrum. *ApJ*, 715:104–121, May 2010. doi: 10.1088/0004-637X/715/1/104.

E. M. Hu, L. L. Cowie, A. J. Barger, P. Capak, Y. Kakazu, and L. Trouille. An Atlas of z = 5.7 and z = 6.5 Lyα Emitters. *ApJ*, 725:394–423, December 2010. doi: 10.1088/0004-637X/725/1/394.

E. M. Hu, L. L. Cowie, A. Songaila, A. J. Barger, B. Rosenwasser, and I. Wold. An Ultraluminous Lyman Alpha Emitter with a Blue Wing at z=6.6. *ArXiv e-prints*, June 2016.

E. Hubble. A Relation between Distance and Radial Velocity among Extra-Galactic Nebulae. *Proceedings of the National Academy of Science*, 15:168–173, March 1929. doi: 10.1073/pnas.15.3.168.

M. Iye, K. Ota, N. Kashikawa, H. Furusawa, T. Hashimoto, T. Hattori, Y. Matsuda, T. Morokuma, M. Ouchi, and K. Shimasaku. A galaxy at

a redshift z = 6.96. *Nature*, 443:186–188, September 2006. doi: 10.1038/nature05104.

W. Karman et al. MUSE integral-field spectroscopy towards the Frontier Fields cluster Abell S1063. I. Data products and redshift identifications. *A&P*, 574:A11, February 2015. doi: 10.1051/0004-6361/201424962.

N. Kashikawa, K. Shimasaku, Y. Matsuda, E. Egami, L. Jiang, T. Nagao, M. Ouchi, M. A. Malkan, T. Hattori, K. Ota, Y. Taniguchi, S. Okamura, C. Ly, M. Iye, H. Furusawa, Y. Shioya, T. Shibuya, Y. Ishizaki, and J. Toshikawa. Completing the Census of Lyα Emitters at the Reionization Epoch. *ApJ*, 734:119, June 2011. doi: 10.1088/0004-637X/734/2/119.

A. A. Khostovan, D. Sobral, B. Mobasher, P. N. Best, I. Smail, J. P. Stott, S. Hemmati, and H. Nayyeri. Evolution of the H β + [O III] and [O II] luminosity functions and the [O II] star formation history of the Universe up to z $\sim$ 5 from HiZELS. *MNRAS*, 452:3948–3968, October 2015. doi: 10.1093/mnras/stv1474.

A. A. Khostovan, D. Sobral, B. Mobasher, I. Smail, B. Darvish, H. Nayyeri, S. Hemmati, and J. P. Stott. The Nature of Hβ+[O{\sc iii}] and [O{\sc ii}] emitters to $z \sim 5$ with HiZELS: stellar mass functions and the evolution of EWs. *ArXiv e-prints*, April 2016.

J.-W. Kim, M. Im, S.-K. Lee, A. C. Edge, D. A. Wake, A. I. Merson, and Y. Jeon. Linking Galaxies to Dark Matter Halos at z ˜ 1 : Dependence of Galaxy Clustering on Stellar Mass and Specific Star Formation Rate. *ApJ*, 806:189, June 2015. doi: 10.1088/0004-637X/806/2/189.

A. A. Klypin and S. F. Shandarin. Three-dimensional numerical model of the formation of large-scale structure in the Universe. *MNRAS*, 204:891–907, September 1983. doi: 10.1093/mnras/204.3.891.

E. Komatsu, J. Dunkley, M. R. Nolta, C. L. Bennett, B. Gold, G. Hinshaw, N. Jarosik, D. Larson, M. Limon, L. Page, D. N. Spergel, M. Halpern, R. S. Hill, A. Kogut, S. S. Meyer, G. S. Tucker, J. L. Weiland, E. Wollack, and E. L. Wright. Five-Year Wilkinson Microwave Anisotropy Probe

Observations: Cosmological Interpretation. *ApJs*, 180:330–376, February 2009. doi: 10.1088/0067-0049/180/2/330.

A. Konno, M. Ouchi, Y. Ono, K. Shimasaku, T. Shibuya, H. Furusawa, K. Nakajima, Y. Naito, R. Momose, S. Yuma, and M. Iye. Accelerated Evolution of the Lyα Luminosity Function at z $\gtrsim$ 7 Revealed by the Subaru Ultra-deep Survey for Lyα Emitters at z = 7.3. *ApJ*, 797:16, December 2014. doi: 10.1088/0004-637X/797/1/16.

A. Konno, M. Ouchi, K. Nakajima, F. Duval, H. Kusakabe, Y. Ono, and K. Shimasaku. Bright and Faint Ends of Lyα Luminosity Functions at z = 2 Determined by the Subaru Survey: Implications for AGNs, Magnification Bias, and ISM H I Evolution. *ApJ*, 823:20, May 2016. doi: 10.3847/0004-637X/823/1/20.

M. Kowalski, D. Rubin, G. Aldering, R. J. Agostinho, A. Amadon, R. Amanullah, C. Balland, K. Barbary, G. Blanc, P. J. Challis, A. Conley, N. V. Connolly, R. Covarrubias, K. S. Dawson, S. E. Deustua, R. Ellis, S. Fabbro, V. Fadeyev, X. Fan, B. Farris, G. Folatelli, B. L. Frye, G. Garavini, E. L. Gates, L. Germany, G. Goldhaber, B. Goldman, A. Goobar, D. E. Groom, J. Haissinski, D. Hardin, I. Hook, S. Kent, A. G. Kim, R. A. Knop, C. Lidman, E. V. Linder, J. Mendez, J. Meyers, G. J. Miller, M. Moniez, A. M. Mourão, H. Newberg, S. Nobili, P. E. Nugent, R. Pain, O. Perdereau, S. Perlmutter, M. M. Phillips, V. Prasad, R. Quimby, N. Regnault, J. Rich, E. P. Rubenstein, P. Ruiz-Lapuente, F. D. Santos, B. E. Schaefer, R. A. Schommer, R. C. Smith, A. M. Soderberg, A. L. Spadafora, L.-G. Strolger, M. Strovink, N. B. Suntzeff, N. Suzuki, R. C. Thomas, N. A. Walton, L. Wang, W. M. Wood-Vasey, and J. L. Yun. Improved Cosmological Constraints from New, Old, and Combined Supernova Data Sets. *ApJ*, 686: 749-778, October 2008. doi: 10.1086/589937.

C. Laigle, H. J. McCracken, O. Ilbert, B. C. Hsieh, I. Davidzon, P. Capak, G. Hasinger, J. D. Silverman, C. Pichon, J. Coupon, H. Aussel, D. Le Borgne, K. Caputi, P. Cassata, Y.-Y. Chang, F. Civano, J. Dunlop, J. Fynbo, J. S. kartaltepe, A. Koekemoer, O. Le Fevre, E. Le Floc'h, A. Leauthaud, S. Lilly, L. Lin, S. Marchesi, B. Milvang-Jensen, M. Salvato, D. B. Sanders, N. Scoville, V. Smolcic, M. Stockmann, Y. Taniguchi,

L. Tasca, S. Toft, M. Vaccari, and J. Zabl. The COSMOS2015 Catalog: Exploring the 1<z<6 Universe with half a million galaxies. *ArXiv e-prints*, April 2016.

A. Lawrence, S. J. Warren, O. Almaini, A. C. Edge, N. C. Hambly, R. F. Jameson, P. Lucas, M. Casali, A. Adamson, S. Dye, J. P. Emerson, S. Foucaud, P. Hewett, P. Hirst, S. T. Hodgkin, M. J. Irwin, N. Lodieu, R. G. McMahon, C. Simpson, I. Smail, D. Mortlock, and M. Folger. The UKIRT Infrared Deep Sky Survey (UKIDSS). *MNRAS*, 379:1599–1617, August 2007. doi: 10.1111/j.1365-2966.2007.12040.x.

G. Lemaître. Un Univers homogène de masse constante et de rayon croissant rendant compte de la vitesse radiale des nébuleuses extra-galactiques. *Annales de la Société Scientifique de Bruxelles*, 47:49–59, 1927.

C. Ly, M. A. Malkan, N. Kashikawa, K. Shimasaku, M. Doi, T. Nagao, M. Iye, T. Kodama, T. Morokuma, and K. Motohara. The Luminosity Function and Star Formation Rate between Redshifts of 0.07 and 1.47 for Narrowband Emitters in the Subaru Deep Field. *ApJ*, 657:738–759, March 2007. doi: 10.1086/510828.

C. Ly, J. C. Lee, D. A. Dale, I. Momcheva, S. Salim, S. Staudaher, C. A. Moore, and R. Finn. The Hα Luminosity Function and Star Formation Rate Volume Density at z = 0.8 from the NEWFIRM Hα Survey. *ApJ*, 726:109, January 2011. doi: 10.1088/0004-637X/726/2/109.

P. Madau. Radiative transfer in a clumpy universe: The colors of high-redshift galaxies. *ApJL*, 441:18–27, March 1995. doi: 10.1086/175332.

P. Madau and M. Dickinson. Cosmic Star-Formation History. *ARAA*, 52: 415–486, August 2014. doi: 10.1146/annurev-astro-081811-125615.

R. Maiolino et al. The assembly of 'normal' galaxies at z $\sim$ 7 probed by ALMA. *MNRAS*, 452:54–68, September 2015. doi: 10.1093/mnras/stv1194.

S. Malhotra and J. E. Rhoads. Luminosity Functions of Lyα Emitters at Redshifts z=6.5 and z=5.7: Evidence against Reionization at z<=6.5. *ApJL*, 617:L5–L8, December 2004. doi: 10.1086/427182.

R. P. Mallery, B. Mobasher, P. Capak, Y. Kakazu, D. Masters, O. Ilbert, S. Hemmati, C. Scarlata, M. Salvato, H. McCracken, O. LeFevre, and N. Scoville. Lyα Emission from High-redshift Sources in COSMOS. *ApJ*, 760:128, December 2012. doi: 10.1088/0004-637X/760/2/128.

M. Markevitch, A. H. Gonzalez, L. David, A. Vikhlinin, S. Murray, W. Forman, C. Jones, and W. Tucker. A Textbook Example of a Bow Shock in the Merging Galaxy Cluster 1E 0657-56. *ApJL*, 567:L27–L31, March 2002. doi: 10.1086/339619.

M. Markevitch, A. H. Gonzalez, D. Clowe, A. Vikhlinin, W. Forman, C. Jones, S. Murray, and W. Tucker. Direct Constraints on the Dark Matter Self-Interaction Cross Section from the Merging Galaxy Cluster 1E 0657-56. *ApJ*, 606:819–824, May 2004. doi: 10.1086/383178.

C. L. Martin and M. Sawicki. The Space Density of Redshift 5.7 Lyα Emitters: First Constraints from a Multislit Windows Search. *ApJ*, 603:414–424, March 2004. doi: 10.1086/381699.

J. Matthee, D. Sobral, S. Santos, H. Röttgering, B. Darvish, and B. Mobasher. Identification of the brightest Lyα emitters at z = 6.6: implications for the evolution of the luminosity function in the reionization era. *MNRAS*, 451:400–417, July 2015. doi: 10.1093/mnras/stv947.

J. Matthee, D. Sobral, P. Best, A. A. Khostovan, I. Oteo, R. Bouwens, and H. Röttgering. The production and escape of Lyman-Continuum radiation from star-forming galaxies at z˜2 and their redshift evolution. *ArXiv e-prints*, May 2016a.

J. Matthee, D. Sobral, I. Oteo, P. Best, I. Smail, H. Röttgering, and A. Paulino-Afonso. The CALYMHA survey: Lyα escape fraction and its dependence on galaxy properties at z=2.23. *MNRAS*, February 2016b. doi: 10.1093/mnras/stw322.

J. J. A. Matthee, D. Sobral, A. M. Swinbank, I. Smail, P. N. Best, J.-W. Kim, M. Franx, B. Milvang-Jensen, and J. Fynbo. A 10 deg^2 Lyman α survey at z=8.8 with spectroscopic follow-up: strong constraints on the luminosity

function and implications for other surveys. *MNRAS*, 440:2375–2387, May 2014. doi: 10.1093/mnras/stu392.

H. J. McCracken, B. Milvang-Jensen, J. Dunlop, M. Franx, J. P. U. Fynbo, O. Le Fèvre, J. Holt, K. I. Caputi, Y. Goranova, F. Buitrago, J. P. Emerson, W. Freudling, P. Hudelot, C. López-Sanjuan, F. Magnard, Y. Mellier, P. Møller, K. K. Nilsson, W. Sutherland, L. Tasca, and J. Zabl. UltraVISTA: a new ultra-deep near-infrared survey in COSMOS. *A&P*, 544: A156, August 2012. doi: 10.1051/0004-6361/201219507.

A. Mesinger. Was reionization complete by z ˜ 5-6? *MNRAS*, 407:1328–1337, September 2010. doi: 10.1111/j.1365-2966.2010.16995.x.

S. Miyazaki, Y. Komiyama, M. Sekiguchi, S. Okamura, M. Doi, H. Furusawa, M. Hamabe, K. Imi, M. Kimura, F. Nakata, N. Okada, M. Ouchi, K. Shimasaku, M. Yagi, and N. Yasuda. Subaru Prime Focus Camera – Suprime-Cam. *PASJ*, 54:833–853, December 2002. doi: 10.1093/pasj/54.6.833.

R. Momose, M. Ouchi, K. Nakajima, Y. Ono, T. Shibuya, K. Shimasaku, S. Yuma, M. Mori, and M. Umemura. Diffuse Lyα haloes around galaxies at z = 2.2-6.6: implications for galaxy formation and cosmic reionization. *MNRAS*, 442:110–120, July 2014. doi: 10.1093/mnras/stu825.

T. Murayama, Y. Taniguchi, N. Z. Scoville, M. Ajiki, D. B. Sanders, B. Mobasher, H. Aussel, P. Capak, A. Koekemoer, Y. Shioya, T. Nagao, C. Carilli, R. S. Ellis, B. Garilli, M. Giavalisco, M. G. Kitzbichler, O. Le Fèvre, D. Maccagni, E. Schinnerer, V. Smolčić, S. Tribiano, A. Cimatti, Y. Komiyama, S. Miyazaki, S. S. Sasaki, J. Koda, and H. Karoji. Lyα Emitters at Redshift 5.7 in the COSMOS Field. *ApJs*, 172:523–544, September 2007. doi: 10.1086/516597.

K. K. Nilsson, P. Møller, O. Möller, J. P. U. Fynbo, M. J. Michałowski, D. Watson, C. Ledoux, P. Rosati, K. Pedersen, and L. F. Grove. A multi-wavelength study of z = 3.15 Lyman-α emitters in the GOODS South Field. *A&P*, 471:71–82, August 2007. doi: 10.1051/0004-6361:20066949.

P. A. Oesch, R. J. Bouwens, G. D. Illingworth, V. Gonzalez, M. Trenti, P. G. van Dokkum, M. Franx, I. Labbé, C. M. Carollo, and D. Magee. The Bright

End of the Ultraviolet Luminosity Function at z ˜ 8: New Constraints from CANDELS Data in GOODS-South. *ApJ*, 759:135, November 2012. doi: 10.1088/0004-637X/759/2/135.

P. A. Oesch, R. J. Bouwens, G. D. Illingworth, I. Labbé, R. Smit, M. Franx, P. G. van Dokkum, I. Momcheva, M. L. N. Ashby, G. G. Fazio, J.-S. Huang, S. P. Willner, V. Gonzalez, D. Magee, M. Trenti, G. B. Brammer, R. E. Skelton, and L. R. Spitler. The Most Luminous z ˜ 9-10 Galaxy Candidates Yet Found: The Luminosity Function, Cosmic Star-formation Rate, and the First Mass Density Estimate at 500 Myr. *ApJ*, 786:108, May 2014. doi: 10.1088/0004-637X/786/2/108.

P. A. Oesch, P. G. van Dokkum, G. D. Illingworth, R. J. Bouwens, I. Momcheva, B. Holden, G. W. Roberts-Borsani, R. Smit, M. Franx, I. Labbé, V. González, and D. Magee. A Spectroscopic Redshift Measurement for a Luminous Lyman Break Galaxy at z = 7.730 Using Keck/MOSFIRE. *ApJL*, 804:L30, May 2015. doi: 10.1088/2041-8205/804/2/L30.

K. Ota, M. Iye, N. Kashikawa, K. Shimasaku, M. Ouchi, T. Totani, M. A. R. Kobayashi, M. Nagashima, A. Harayama, N. Kodaka, T. Morokuma, H. Furusawa, A. Tajitsu, and T. Hattori. Lyα Emitters at z = 7 in the Subaru/XMM-Newton Deep Survey Field: Photometric Candidates and Luminosity Functions. *ApJ*, 722:803–811, October 2010. doi: 10.1088/0004-637X/722/1/803.

M. Ouchi, K. Shimasaku, S. Okamura, H. Furusawa, N. Kashikawa, K. Ota, M. Doi, M. Hamabe, M. Kimura, Y. Komiyama, M. Miyazaki, S. Miyazaki, F. Nakata, M. Sekiguchi, M. Yagi, and N. Yasuda. Subaru Deep Survey. V. A Census of Lyman Break Galaxies at z˜=4 and 5 in the Subaru Deep Fields: Photometric Properties. *ApJ*, 611:660–684, August 2004. doi: 10.1086/422207.

M. Ouchi, K. Shimasaku, M. Akiyama, C. Simpson, T. Saito, Y. Ueda, H. Furusawa, K. Sekiguchi, T. Yamada, T. Kodama, N. Kashikawa, S. Okamura, M. Iye, T. Takata, M. Yoshida, and M. Yoshida. The Subaru/XMM-Newton Deep Survey (SXDS). IV. Evolution of Lyα Emitters from z=3.1

to 5.7 in the 1 deg^2 Field: Luminosity Functions and AGN. *ApJs*, 176: 301–330, June 2008. doi: 10.1086/527673.

M. Ouchi, K. Shimasaku, H. Furusawa, T. Saito, M. Yoshida, M. Akiyama, Y. Ono, T. Yamada, K. Ota, N. Kashikawa, M. Iye, T. Kodama, S. Okamura, C. Simpson, and M. Yoshida. Statistics of 207 Lyα Emitters at a Redshift Near 7: Constraints on Reionization and Galaxy Formation Models. *ApJ*, 723:869–894, November 2010. doi: 10.1088/0004-637X/723/1/869.

M. Ouchi, R. Ellis, Y. Ono, K. Nakanishi, K. Kohno, R. Momose, Y. Kurono, M. L. N. Ashby, K. Shimasaku, S. P. Willner, G. G. Fazio, Y. Tamura, and D. Iono. An Intensely Star-forming Galaxy at z ˜ 7 with Low Dust and Metal Content Revealed by Deep ALMA and HST Observations. *ApJ*, 778:102, December 2013. doi: 10.1088/0004-637X/778/2/102.

R. B. Partridge and P. J. E. Peebles. Are Young Galaxies Visible? *ApJ*, 147: 868, March 1967. doi: 10.1086/149079.

P. J. E. Peebles. Recombination of the Primeval Plasma. *ApJ*, 153:1, July 1968. doi: 10.1086/149628.

L. Pentericci, E. Vanzella, A. Fontana, M. Castellano, T. Treu, A. Mesinger, M. Dijkstra, A. Grazian, M. Bradač, C. Conselice, S. Cristiani, J. Dunlop, A. Galametz, M. Giavalisco, E. Giallongo, A. Koekemoer, R. McLure, R. Maiolino, D. Paris, and P. Santini. New Observations of z ˜ 7 Galaxies: Evidence for a Patchy Reionization. *ApJ*, 793:113, October 2014. doi: 10.1088/0004-637X/793/2/113.

A. A. Penzias and R. W. Wilson. A Measurement of Excess Antenna Temperature at 4080 Mc/s. *ApJ*, 142:419–421, July 1965. doi: 10.1086/148307.

P. G. Pérez-González, A. Cava, G. Barro, V. Villar, N. Cardiel, I. Ferreras, J. M. Rodríguez-Espinosa, A. Alonso-Herrero, M. Balcells, J. Cenarro, J. Cepa, S. Charlot, A. Cimatti, C. J. Conselice, E. Daddi, J. Donley, D. Elbaz, N. Espino, J. Gallego, R. Gobat, O. González-Martín, R. Guzmán, A. Hernán-Caballero, C. Muñoz-Tuñón, A. Renzini, J. Rodríguez-Zaurín,

L. Tresse, I. Trujillo, and J. Zamorano. SHARDS: An Optical Spectrophotometric Survey of Distant Galaxies. *ApJ*, 762:46, January 2013. doi: 10.1088/0004-637X/762/1/46.

S. Perlmutter, G. Aldering, G. Goldhaber, R. A. Knop, P. Nugent, P. G. Castro, S. Deustua, S. Fabbro, A. Goobar, D. E. Groom, I. M. Hook, A. G. Kim, M. Y. Kim, J. C. Lee, N. J. Nunes, R. Pain, C. R. Pennypacker, R. Quimby, C. Lidman, R. S. Ellis, M. Irwin, R. G. McMahon, P. Ruiz-Lapuente, N. Walton, B. Schaefer, B. J. Boyle, A. V. Filippenko, T. Matheson, A. S. Fruchter, N. Panagia, H. J. M. Newberg, W. J. Couch, and T. S. C. Project. Measurements of Ω and Λ from 42 High-Redshift Supernovae. *ApJ*, 517:565–586, June 1999. doi: 10.1086/307221.

Planck Collaboration, P. A. R. Ade, N. Aghanim, M. Arnaud, M. Ashdown, J. Aumont, C. Baccigalupi, A. J. Banday, R. B. Barreiro, J. G. Bartlett, and et al. Planck 2015 results. XIII. Cosmological parameters. *ArXiv e-prints*, February 2015.

C. J. Pritchet. The search for primeval galaxies. *PASP*, 106:1052–1067, October 1994. doi: 10.1086/133479.

M. Rauch, M. Haehnelt, A. Bunker, G. Becker, F. Marleau, J. Graham, S. Cristiani, M. Jarvis, C. Lacey, S. Morris, C. Peroux, H. Röttgering, and T. Theuns. A Population of Faint Extended Line Emitters and the Host Galaxies of Optically Thick QSO Absorption Systems. *ApJ*, 681:856–880, July 2008. doi: 10.1086/525846.

J. E. Rhoads, S. Malhotra, A. Dey, D. Stern, H. Spinrad, and B. T. Jannuzi. First Results from the Large-Area Lyman Alpha Survey. *ApJL*, 545:L85–L88, December 2000. doi: 10.1086/317874.

J. E. Rhoads, A. Dey, S. Malhotra, D. Stern, H. Spinrad, B. T. Jannuzi, S. Dawson, M. J. I. Brown, and E. Landes. Spectroscopic Confirmation of Three Redshift z˜5.7 Lyα Emitters from the Large-Area Lyman Alpha Survey. *AJ*, 125:1006–1013, March 2003. doi: 10.1086/346272.

A. G. Riess, A. V. Filippenko, P. Challis, A. Clocchiatti, A. Diercks, P. M. Garnavich, R. L. Gilliland, C. J. Hogan, S. Jha, R. P. Kirshner, B. Lei-

bundgut, M. M. Phillips, D. Reiss, B. P. Schmidt, R. A. Schommer, R. C. Smith, J. Spyromilio, C. Stubbs, N. B. Suntzeff, and J. Tonry. Observational Evidence from Supernovae for an Accelerating Universe and a Cosmological Constant. *AJ*, 116:1009–1038, September 1998. doi: 10.1086/300499.

B. E. Robertson, R. S. Ellis, J. S. Dunlop, R. J. McLure, and D. P. Stark. Early star-forming galaxies and the reionization of the Universe. *Nature*, 468:49–55, November 2010. doi: 10.1038/nature09527.

S. Santos, D. Sobral, and J. Matthee. The Lyman-alpha luminosity function at z=5.7-6.6 and the steep drop of the faint end: implications for reionization. *ArXiv e-prints*, June 2016.

M. Sawicki et al. The DEEP2 Redshift Survey: Lyα Emitters in the Spectroscopic Database. *ApJ*, 687:884-898, November 2008. doi: 10.1086/591779.

D. Schaerer, F. Boone, M. Zamojski, J. Staguhn, M. Dessauges-Zavadsky, S. Finkelstein, and F. Combes. New constraints on dust emission and UV attenuation of z = 6.5-7.5 galaxies from millimeter observations. *A&A*, 574:A19, February 2015. doi: 10.1051/0004-6361/201424649.

P. Schechter. An analytic expression for the luminosity function for galaxies. *ApJ*, 203:297–306, January 1976. doi: 10.1086/154079.

M. A. Schenker, R. S. Ellis, N. P. Konidaris, and D. P. Stark. Line-emitting Galaxies beyond a Redshift of 7: An Improved Method for Estimating the Evolving Neutrality of the Intergalactic Medium. *ApJ*, 795:20, November 2014. doi: 10.1088/0004-637X/795/1/20.

K. B. Schmidt et al. The Grism Lens-Amplified Survey from Space (GLASS). III. A Census of Lyα Emission at z $gtrsim$ 7 from HST Spectroscopy. *ApJ*, 818:38, February 2016. doi: 10.3847/0004-637X/818/1/38.

C. K. Seyfert. Nuclear Emission in Spiral Nebulae. *ApJ*, 97:28, January 1943. doi: 10.1086/144488.

T. Shibuya, N. Kashikawa, K. Ota, M. Iye, M. Ouchi, H. Furusawa, K. Shimasaku, and T. Hattori. The First Systematic Survey for Lyα Emitters

at z = 7.3 with Red-sensitive Subaru/Suprime-Cam. *ApJ*, 752:114, June 2012. doi: 10.1088/0004-637X/752/2/114.

K. Shimasaku, N. Kashikawa, M. Doi, C. Ly, M. A. Malkan, Y. Matsuda, M. Ouchi, T. Hayashino, M. Iye, K. Motohara, T. Murayama, T. Nagao, K. Ohta, S. Okamura, T. Sasaki, Y. Shioya, and Y. Taniguchi. Lyα Emitters at z = 5.7 in the Subaru Deep Field. *PASJ*, 58:313–334, April 2006. doi: 10.1093/pasj/58.2.313.

M. F. Skrutskie, R. M. Cutri, R. Stiening, M. D. Weinberg, S. Schneider, J. M. Carpenter, C. Beichman, R. Capps, T. Chester, J. Elias, J. Huchra, J. Liebert, C. Lonsdale, D. G. Monet, S. Price, P. Seitzer, T. Jarrett, J. D. Kirkpatrick, J. E. Gizis, E. Howard, T. Evans, J. Fowler, L. Fullmer, R. Hurt, R. Light, E. L. Kopan, K. A. Marsh, H. L. McCallon, R. Tam, S. Van Dyk, and S. Wheelock. The Two Micron All Sky Survey (2MASS). *AJ*, 131:1163–1183, February 2006. doi: 10.1086/498708.

J. Smidt, B. K. Wiggins, and J. L. Johnson. Ab Initio Cosmological Simulations of CR7 as an Active Black Hole. *ArXiv e-prints*, March 2016.

A. Smith, V. Bromm, and A. Loeb. Evidence for a direct collapse black hole in the Lyman-alpha source CR7. *ArXiv e-prints*, February 2016.

G. F. Smoot, C. L. Bennett, A. Kogut, E. L. Wright, J. Aymon, N. W. Boggess, E. S. Cheng, G. de Amici, S. Gulkis, M. G. Hauser, G. Hinshaw, P. D. Jackson, M. Janssen, E. Kaita, T. Kelsall, P. Keegstra, C. Lineweaver, K. Loewenstein, P. Lubin, J. Mather, S. S. Meyer, S. H. Moseley, T. Murdock, L. Rokke, R. F. Silverberg, L. Tenorio, R. Weiss, and D. T. Wilkinson. Structure in the COBE differential microwave radiometer first-year maps. *ApJL*, 396:L1–L5, September 1992. doi: 10.1086/186504.

D. Sobral, P. N. Best, J. E. Geach, I. Smail, J. Kurk, M. Cirasuolo, M. Casali, R. J. Ivison, K. Coppin, and G. B. Dalton. Bright Lyα emitters at z ˜ 9: constraints on the LF from HizELS. *MNRAS*, 398:L68–L72, September 2009. doi: 10.1111/j.1745-3933.2009.00712.x.

D. Sobral, P. N. Best, Y. Matsuda, I. Smail, J. E. Geach, and M. Cirasuolo. Star formation at z=1.47 from HiZELS: an H$\gtrsim\alpha$+[O II] double-blind

study. *MNRAS*, 420:1926–1945, March 2012. doi: 10.1111/j.1365-2966.2011.19977.x.

D. Sobral, I. Smail, P. N. Best, J. E. Geach, Y. Matsuda, J. P. Stott, M. Cirasuolo, and J. Kurk. A large Hα survey at z = 2.23, 1.47, 0.84 and 0.40: the 11 Gyr evolution of star-forming galaxies from HiZELS. *MNRAS*, 428:1128–1146, January 2013. doi: 10.1093/mnras/sts096.

D. Sobral, J. Matthee, B. Darvish, D. Schaerer, B. Mobasher, H. J. A. Röttgering, S. Santos, and S. Hemmati. Evidence for PopIII-like Stellar Populations in the Most Luminous Lyman-α Emitters at the Epoch of Reionization: Spectroscopic Confirmation. *ApJ*, 808:139, August 2015. doi: 10.1088/0004-637X/808/2/139.

D. N. Spergel, L. Verde, H. V. Peiris, E. Komatsu, M. R. Nolta, C. L. Bennett, M. Halpern, G. Hinshaw, N. Jarosik, A. Kogut, M. Limon, S. S. Meyer, L. Page, G. S. Tucker, J. L. Weiland, E. Wollack, and E. L. Wright. First-Year Wilkinson Microwave Anisotropy Probe (WMAP) Observations: Determination of Cosmological Parameters. *ApJs*, 148:175–194, September 2003. doi: 10.1086/377226.

D. N. Spergel, R. Bean, O. Doré, M. R. Nolta, C. L. Bennett, J. Dunkley, G. Hinshaw, N. Jarosik, E. Komatsu, L. Page, H. V. Peiris, L. Verde, M. Halpern, R. S. Hill, A. Kogut, M. Limon, S. S. Meyer, N. Odegard, G. S. Tucker, J. L. Weiland, E. Wollack, and E. L. Wright. Three-Year Wilkinson Microwave Anisotropy Probe (WMAP) Observations: Implications for Cosmology. *ApJs*, 170:377–408, June 2007. doi: 10.1086/513700.

V. Springel, S. D. M. White, A. Jenkins, C. S. Frenk, N. Yoshida, L. Gao, J. Navarro, R. Thacker, D. Croton, J. Helly, J. A. Peacock, S. Cole, P. Thomas, H. Couchman, A. Evrard, J. Colberg, and F. Pearce. Simulations of the formation, evolution and clustering of galaxies and quasars. *Nature*, 435:629–636, June 2005. doi: 10.1038/nature03597.

D. P. Stark, R. S. Ellis, J. Richard, J.-P. Kneib, G. P. Smith, and M. R. Santos. A Keck Survey for Gravitationally Lensed Lyα Emitters in the

Redshift Range 8.5<z<10.4: New Constraints on the Contribution of Low-Luminosity Sources to Cosmic Reionization. *ApJj*, 663:10–28, July 2007. doi: 10.1086/518098.

D. P. Stark, R. S. Ellis, K. Chiu, M. Ouchi, and A. Bunker. Keck spectroscopy of faint 3 < z < 7 Lyman break galaxies - I. New constraints on cosmic reionization from the luminosity and redshift-dependent fraction of Lyman α emission. *MNRAS*, 408:1628–1648, November 2010. doi: 10.1111/j.1365-2966.2010.17227.x.

D. P. Stark et al. Lyman-alpha and CIII] Emission in z=7-9 Galaxies: Accelerated Reionization Around Luminous Star Forming Systems? *ArXiv e-prints*, June 2016.

C. C. Steidel, M. Giavalisco, M. Dickinson, and K. L. Adelberger. Spectroscopy of Lyman Break Galaxies in the Hubble Deep Field. *AJ*, 112:352, August 1996. doi: 10.1086/118019.

C. C. Steidel, M. Bogosavljević, A. E. Shapley, J. A. Kollmeier, N. A. Reddy, D. K. Erb, and M. Pettini. Diffuse Lyα Emitting Halos: A Generic Property of High-redshift Star-forming Galaxies. *ApJ*, 736:160, August 2011. doi: 10.1088/0004-637X/736/2/160.

M. I. Takahashi, Y. Shioya, Y. Taniguchi, T. Murayama, M. Ajiki, S. S. Sasaki, O. Koizumi, T. Nagao, N. Z. Scoville, B. Mobasher, H. Aussel, P. Capak, C. Carilli, R. S. Ellis, B. Garilli, M. Giavalisco, L. Guzzo, G. Hasinger, C. Impey, M. G. Kitzbichler, A. Koekemoer, O. Le Fèvre, S. J. Lilly, D. Maccagni, A. Renzini, M. Rich, D. B. Sanders, E. Schinnerer, M. Scodeggio, P. Shopbell, V. Smolčić, S. Tribiano, Y. Ideue, and S. Mihara. The [O II] λ3727 Luminosity Function and Star Formation Rate at z˜1.2 in the COSMOS 2 Square Degree Field and the Subaru Deep Field. *ApJs*, 172:456–467, September 2007. doi: 10.1086/518037.

Y. Taniguchi et al. The SUBARU Deep Field Project: Lymanα Emitters at a Redshift of 6.6. *PASJ*, 57:165–182, February 2005. doi: 10.1093/pasj/57.1.165.

Y. Taniguchi et al. The Cosmic Evolution Survey (COSMOS): Subaru Observations of the HST Cosmos Field. *ApJS*, 172:9–28, September 2007. doi: 10.1086/516596.

M. B. Taylor. STILTS - A Package for Command-Line Processing of Tabular Data. In C. Gabriel, C. Arviset, D. Ponz, and S. Enrique, editors, *Astronomical Data Analysis Software and Systems XV*, volume 351 of *Astronomical Society of the Pacific Conference Series*, page 666, July 2006.

M. Tegmark, J. Silk, M. J. Rees, A. Blanchard, T. Abel, and F. Palla. How Small Were the First Cosmological Objects? *ApJ*, 474:1, January 1997. doi: 10.1086/303434.

C. van Breukelen, M. J. Jarvis, and B. P. Venemans. The luminosity function of Lyα emitters at $2.3 < z < 4.6$ from integral-field spectroscopy*. *MNRAS*, 359:895–905, May 2005. doi: 10.1111/j.1365-2966.2005.08916.x.

E. Visbal, Z. Haiman, and G. L. Bryan. Formation of Massive Population III Galaxies through Photoionization Feedback: A Possible Explanation for CR7. *MNRAS*, April 2016. doi: 10.1093/mnrasl/slw071.

S. J. Warren et al. The UKIRT Infrared Deep Sky Survey Second Data Release. *arXiv:0703037*, March 2007.

D. Watson, L. Christensen, K. K. Knudsen, J. Richard, A. Gallazzi, and M. J. Michałowski. A dusty, normal galaxy in the epoch of reionization. *Nature*, 519:327–330, March 2015. doi: 10.1038/nature14164.

M. Weidinger, P. Møller, J. P. U. Fynbo, and B. Thomsen. The extended Lyman-α emission surrounding the z = 3.04 radio-quiet QSO1205-30: Primordial infalling gas illuminated by the quasar? *AAP*, 436:825–835, June 2005. doi: 10.1051/0004-6361:20042304.

S. Weinberg. The cosmological constant problem. *Reviews of Modern Physics*, 61:1–23, January 1989. doi: 10.1103/RevModPhys.61.1.

E. Westra, D. H. Jones, C. E. Lidman, K. Meisenheimer, R. M. Athreya, C. Wolf, T. Szeifert, E. Pompei, and L. Vanzi. The wide field imager Lyman-alpha search (WFILAS) for galaxies at redshift ˜5.7. II. Survey

design and sample analysis. *A&P*, 455:61–72, August 2006. doi: 10.1051/0004-6361:20064882.

C. J. Willott, P. Delorme, C. Reylé, L. Albert, J. Bergeron, D. Crampton, X. Delfosse, T. Forveille, J. B. Hutchings, R. J. McLure, A. Omont, and D. Schade. The Canada-France High-z Quasar Survey: Nine New Quasars and the Luminosity Function at Redshift 6. *AJ*, 139:906–918, March 2010. doi: 10.1088/0004-6256/139/3/906.

L. Wisotzki, R. Bacon, J. Blaizot, J. Brinchmann, E. C. Herenz, J. Schaye, N. Bouché, S. Cantalupo, T. Contini, C. M. Carollo, J. Caruana, J.-B. Courbot, E. Emsellem, S. Kamann, J. Kerutt, F. Leclercq, S. J. Lilly, V. Patrício, C. Sandin, M. Steinmetz, L. A. Straka, T. Urrutia, A. Verhamme, P. M. Weilbacher, and M. Wendt. Extended Lyman α haloes around individual high-redshift galaxies revealed by MUSE. *A&P*, 587: A98, March 2016. doi: 10.1051/0004-6361/201527384.

J. Zabl, H. U. Nørgaard-Nielsen, J. P. U. Fynbo, P. Laursen, M. Ouchi, and P. Kjærgaard. Deep rest-frame far-UV spectroscopy of the giant Lyman α emitter 'Himiko'. *MNRAS*, 451:2050–2070, August 2015. doi: 10.1093/mnras/stv1019.

A. Zitrin, I. Labbé, S. Belli, R. Bouwens, R. S. Ellis, G. Roberts-Borsani, D. P. Stark, P. A. Oesch, and R. Smit. Lymanα Emission from a Luminous z = 8.68 Galaxy: Implications for Galaxies as Tracers of Cosmic Reionization. *ApJL*, 810:L12, September 2015. doi: 10.1088/2041-8205/810/1/L12.

Acknowledgments

This work was performed with financial support obtained by Sérgio Santos, David Sobral and Jorryt Matthee.

The authors acknowledge financial support from the Netherlands Organisation for Scientific research (NWO) through a Veni fellowship. Sérgio Santos and David Sobral acknowledge funding from FCT through a FCT Investigator Starting Grant and Start-up Grant (IF/01154/2012/CP0189/CT0010). Sérgio Santos also acknowledges support from FCT through the research grants UID/FIS/04434/2013 and PTDC/FIS-AST/2194/2012. Jorryt Matthee acknowledges a Huygens PhD fellowship from Leiden University.

Based on observations with the Subaru Telescope (Program IDs: S05B-027, S06A-025, S06B-010, S07A-013, S07B-008, S08B-008, S09A-017, S14A-086). Based on observations made with ESO Telescopes at the La Silla Paranal Observatory under programme ID 294.A-5018. Based on observations obtained with MegaPrime/Megacam, a joint project of CFHT and CEA/IRFU, at the Canada-France-Hawaii Telescope (CFHT) which is operated by the National Research Council (NRC) of Canada, the Institut National des Science de l'Univers of the Centre National de la Recherche Scientifique (CNRS) of France, and the University of Hawaii. This work is based in part on data products produced at Terapix available at the Canadian Astronomy Data Centre as part of the Canada-France-Hawaii Telescope Legacy Survey, a collaborative project of NRC and CNRS. Based on data products from observations made with ESO Telescopes at the La Silla Paranal Observatory under ESO programme ID 179.A-2005 and on data products produced by TERAPIX and the Cambridge Astronomy Survey Unit on behalf of the UltraVISTA consortium. We are grateful to the CFHTLS, COSMOS-UltraVISTA, UKIDSS, SXDF and COSMOS survey teams. Without these

legacy surveys, this research would have been impossible.

The authors wish to recognize and acknowledge the very significant cultural role and reverence that the summit of Mauna Kea has always had within the indigenous Hawaiian community. We are most fortunate to have the opportunity to conduct and explore observations from this mountain.

Finally, the authors acknowledge the unique value of the publicly available programming language PYTHON, including the NUMPY, PYFITS, MATPLOTLIB, SCIPY and ASTROPY (Astropy Collaboration et al., 2013) packages.

Personal acknowledgments

There are a lot of people I wish to thank and without whom this dissertation would not have been possible.

I will start by thanking my supervisor, David Sobral, for all the guidance in the past three years, from the final bachelor project. These past years have been a sea of opportunities, with observations in world leading telescopes, collaborations in other universities throughout Europe, international conferences, scientific publications, press releases, etc, etc... None of these would have been possible without your constant support and encouragement and I am eternally grateful for that.

I want to give a huge thank you to Jorryt Matthee, for all your patience throughout this entire work. Without your countless feedback and help I would have never been able to get this far. I am truly thankful that you kept me from going insane.

I want to thank the director of IA, Dr. José Afonso, for providing me with all the resources and infrastructure essential to complete this dissertation. I also want to thank the coordinator of the MSc in Physics, Dr. Iveta Pimentel, for always standing up to protect the students rights and wishes.

I couldn't possibly do an acknowledgement without thanking my family. Firstly, my mother for supporting me every step of the way and giving me the freedom to do what I love. My grandmother for being the backbone of the family. My sister for being the role model that I want to follow. And of course, Ulisses and Mel, for being there for my sister.

Rosa, for being the beacon of light that warms my hearth. For your undeniable support and for always believing in me.

To my office mates and colleagues, Ruben e Miguel: we followed a tough path but it seems we are reaching our goal. Same for Alex, Diogo, Manuel, Azinheira and Miguel Martins, even though we ended up going for different goals.

To my predecessors who passed the MSc trial a few years ago, João and Ana, for all the wisdom and support that you have shared with this rookie. I hope I filled your shoes well. Also, João, for all your sarcastic humour that always lightens up my day.

Lastly, a thank you to all my long time friends, for keeping our brotherhood united. Tiago, César, Paixão, Pedro, Moura e Hugo, I hope this friendship lasts throughout the ages!

This dissertation is dedicated to all those who are not here any more but will always be present.

Appendix A

Lyman series

Hydrogen (H) is the first chemical element of the periodic table. It is the most abundant element of the Universe and was first formed at the time of the Big Bang. Large amounts of hydrogen reside in both the ISM (Inter-stellar medium) and IGM (Inter-galactic medium), which greatly influences how radiation in galaxies is emitted and what escapes. It is essential to understand this element - in particular the key mechanisms behind the production of emission lines - in order to have a clearer image on how galaxies form and evolve.

An atom of hydrogen is composed by a positive nucleus (one proton and one neutron) and one electron which orbits around the nucleus. According to the Bohr model of the atom, the electron can occupy orbits with well defined energetic values. Each orbit is defined by a principal quantum number ($n = 1, 2, 3, ...$), with $n = 1$ being the ground-state. If the atom absorbs energy (e.g. in form of radiation), the electron will transit to a higher orbital number. When the electron returns to the ground-state, it will emit energy in the form of radiation.

The Planck-Einstein equation relates the energy (E) of a photon with its wavelength λ:

$$E = h\frac{c}{\lambda} \tag{A.1}$$

Where h is the Planck constant and c the speed of light.

As the orbits have well defined energies, this radiation will be emitted at specific wavelengths given by the value of the initial (n_i) and final (n_f)

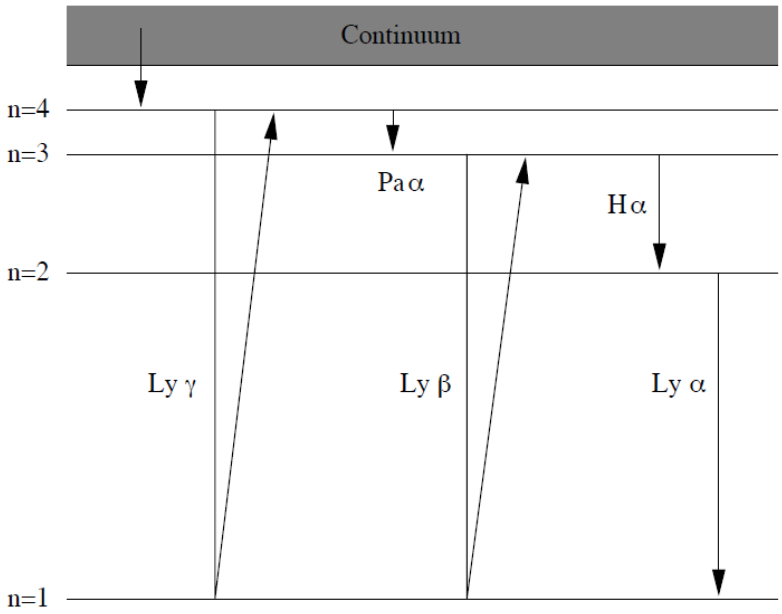

Figure A.1: Illustration of some recombination lines from the hydrogen atom. Hα and Lyα are some of the most common transitions, resulting in strong lines.

orbits. This emission at specific wavelengths is known as an emission line. The wavelength of the radiation emitted for each transition can be calculated with the Rydberg equation:

$$\frac{1}{\lambda} = R_H \left(\frac{1}{n_f^2} - \frac{1}{n_i^2} \right) \tag{A.2}$$

Where $R_H = 1.10 \times 10^7$ m^{-1} is the Rydberg constant for the hydrogen atom.

Lyman series is the set of transitions from $n_i \geq 2$ to the ground-state, $n_f = 1$. In Figure A.1 we show some transitions from the Lyman series. For each hydrogen series, the transitions are named with greek letters, starting with the lowest energy transition (e.g. Lyman-α) and followed by the subsequently more energetic transitions (e.g. Lyman-β, Lyman-γ, ...).

The lowest energy transition from the Lyman series, Lyman-α (transition of the electron from $n = 2$ to $n = 1$), results in the emission of radiation with

$\lambda = 1215.67$ Å (rest-frame UV). Lyman-α is the most common transition as electrons usually do not directly drop from a high energy orbit to the ground-state. Instead, there is typically a sequence of low energy transitions that ends with a final passage from $n = 2$ to $n = 1$. This makes Lyman-α intrinsically one of the strongest recombination lines in the spectra of a star-forming galaxy. This line is the focus of our study.

The energy of the emitted radiation increases with n_i. The upper limit, know as the Lyman limit, corresponds to $n_i = \infty$, which translates to $\lambda = 912$ Å. This is the energy necessary to strip an electron from the atom by photoelectric effect. Radiation more energetic than 912 Å will thus ionize hydrogen atoms.